Table 1. T_g of Nifedipine–PVP and Phenobarbital–PVP Solid Dispersions

	T_g (°C)[a]
Nifedipine	41.9 ± 0.4
Nifedipine–PVP 90:10	43.5 ± 1.0
Nifedipine–PVP 80:20	51.9 ± 0.1
Nifedipine–PVP 70:30	69.5 ± 0.8
Nifedipine–PVP 50:50	96.9 ± 0.4
Nifedipine–PVP 30:70	124.9 ± 0.7
Phenobarbital	40.8 ± 0.2
Phenobarbital–PVP 90:10	46.5 ± 0.1
Phenobarbital–PVP 80:20	57.7 ± 0.2
Phenobarbital–PVP 65:35	89.6 ± 0.5
Phenobarbital–PVP 50:50	115.3 ± 0.9
Phenobarbital–PVP 70:30	135.5 ± 0.6
PVP	168.2 ± 0.6

[a]Average and standard deviation of the mid-point T_g ($n = 3$).

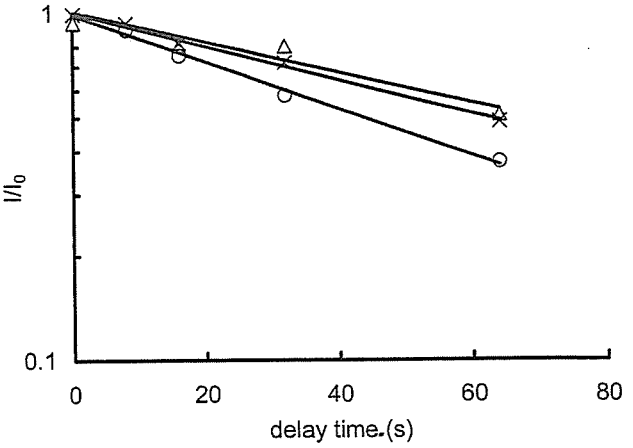

Figure 1. Typical signal decay of the PVP carbonyl carbon. ○, pure PVP; △, nifedipine–PVP (8:2); ×, phenobarbital–PVP (8:2).

^{13}C High-Resolution Solid State NMR

NMR measurements were carried out using freshly prepared samples in order to minimize the possible effect of enthalpy relaxation on the T_1. The amorphous samples obtained were very gently pulverized by using a spatula and, avoiding mechanical stress, put into NMR rotors. The NMR sample preparation was carried out in a grove bag filled with dry nitrogen in order to avoid water sorption by samples. The water content of the samples was determined to be less than 0.1 w/w% by the Karl–Fisher method. NMR measurements were carried out at 27°C with a Varian Unity plus spectrometer (Varian, Inc., Palo Alto, CA) at a proton resonance frequency of 400 MHz. The chemical shift calibration of the instrument was conducted with hexamethylbenzene (methyl group at 17.3 ppm) as an external standard. The pulse sequence for T_1 measurement was that reported by Torchia.[25] The spinning rate was 6.5 kHz, the contact time was 1 ms, delay time was 0.1, 8, 16, 32, 64 s, and recycling delay was 5 s. Scans (400–500) were accumulated for each spectrum. Signals were assigned according to chemical shift data reported for PVP, nicardipine, nimodipine, nifedipine, and phenobarbital glucoside.[19,26–30] Nifedipine carbons observed at 103 ppm were assigned to be C-2 and C-6 carbons[26,27] or C-3 and C-5 carbons.[29] Figure 1 shows the typical signal decay of the PVP carbonyl carbon. When the PVP carbonyl group interacts with drugs, signal decay is expected to be describable by the sum of two or more exponential functions, since there are at least two types of PVP carbonyl carbons with different molecular mobilities. It was, however, difficult to separate the signal decay into two exponential functions, since differences in T_1 were small, as shown in Figure 1. Therefore, the signal decay of all carbons was described by a single exponential function and apparent T_1 values were reported in this paper. There was no significant change in DSC thermograms, suggesting no crystallization occurring in the solid dispersion samples after NMR measurements.

RESULTS AND DISCUSSION

Effect of Drug Content on Chemical Shift and T_1 of PVP Carbons

Figures 2 and 3 show typical ^{13}C-CP/MAS NMR spectra of nifedipine–PVP and phenobarbital–PVP solid dispersions. The chemical shift of the PVP carbonyl carbon, observed at approximately 175 ppm, increased in the presence of nifedipine or phenobarbital. For the phenobarbital–PVP solid dispersion, the chemical shift of C-2 carbon of PVP decreased from 19.5 ± 0.1 ppm to 19.0 ± 0.2 ppm. In contrast, the chemical shift of PVP carbons other than the carbonyl carbon did not change within experimental error for the nifedipine–PVP solid dispersions. Figure 4 shows the effects of drug content on the chemical shift of the PVP carbonyl carbon. The chemical shift

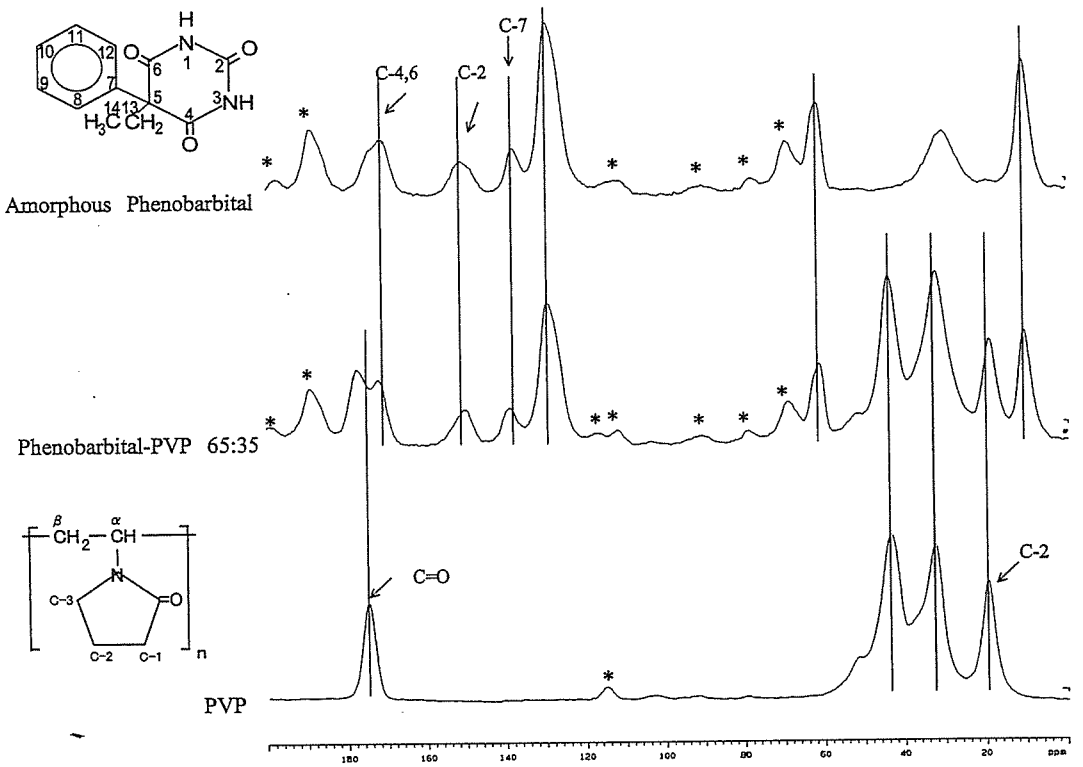

Figure 2. Typical ^{13}C CP/MAS spectra of amorphous phenobarbital–PVP. * represents spining side bands.

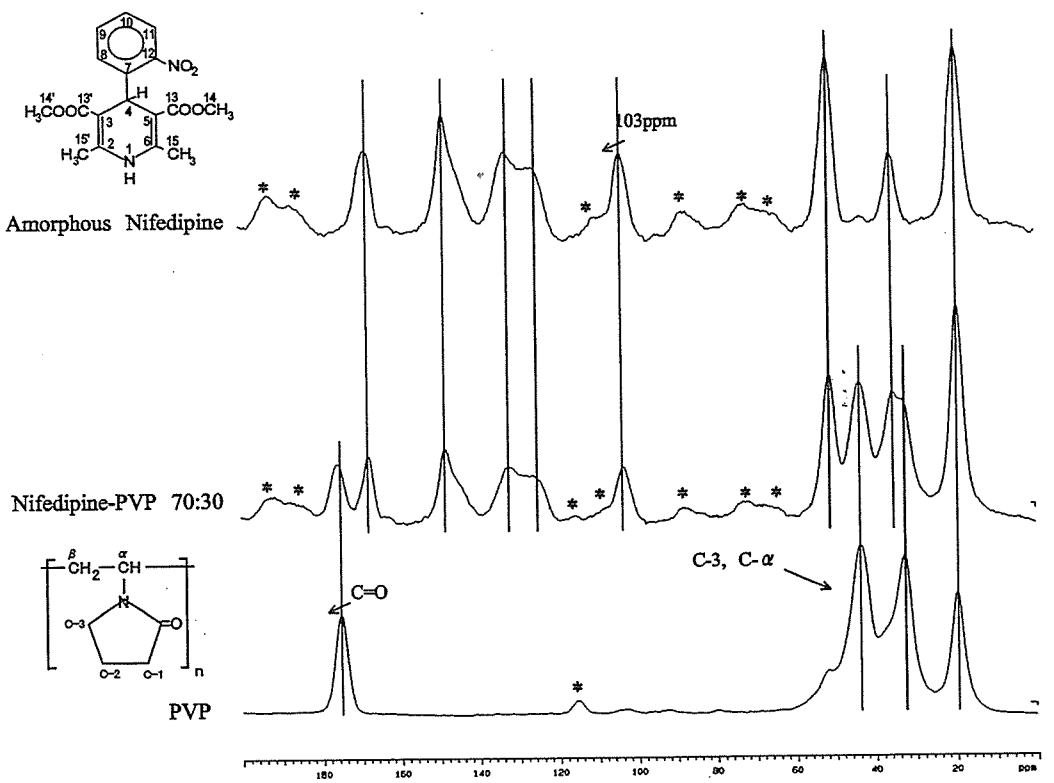

Figure 3. Typical ^{13}C CP/MAS spectra of amorphous nifedipine–PVP. * represents spining side bands.

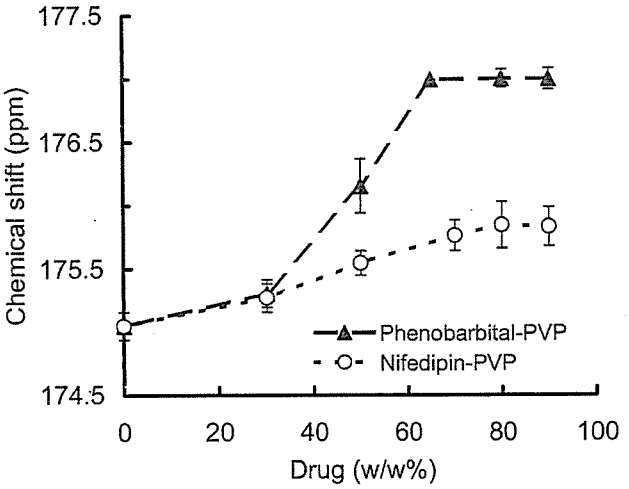

Figure 4. Effect of phenobarbital and nifedipine on the chemical shift of the PVP carbonyl carbon. Error bars represent standard deviation ($n = 3$).

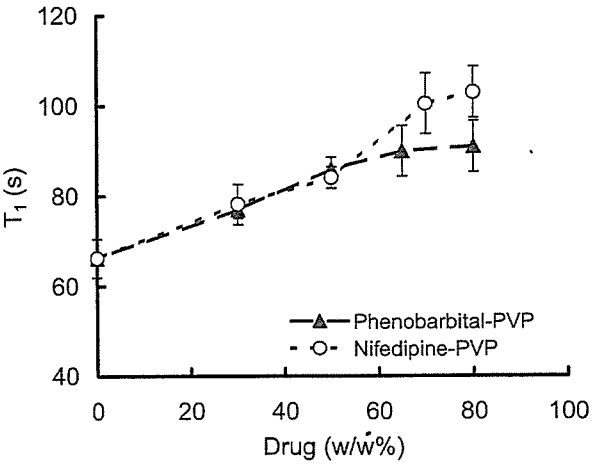

Figure 5. Effect of phenobarbital and nifedipine on the T_1 of the PVP carbonyl carbon. Error bars represent standard deviation ($n = 3$).

increased as the drug content increased and appeared to reach a plateau at a nifedipine content of approximately 70 w/w% or a phenobarbital content of approximately 65 w/w%. These drug contents correspond to a molar ratio of drug to PVP monomer unit of 1:1. The increases in the chemical shift of PVP carbon (more than 1 ppm) was larger than those observed for other PVP carbons (less than 0.5 ppm). It has been reported that the chemical shift of the carbonyl carbon of poly(3-hydroxybutyrate) (PHB) increases by approximately 1 ppm in the presence of polyvinyl alcohol (PVA), indicating changes in the electronic environment of the carbonyl carbon resulting from hydrogen bonding between the carbonyl group of PHB and the hydroxyl group of PVA.[23] Further, hydrogen bond interaction between the PVP carbonyl group and the nifedipine NH group has been indicated by FT–IR spectroscopy.[11] Therefore, the increases in chemical shift of the PVP carbonyl carbon observed in this study suggests hydrogen bond interactions between the PVP carbonyl group and a hydrogen donor group (NH group) from the drug, in a similar manner to the PHB-PVA systems.

Figure 5 shows the effects of drug content on the T_1 of the PVP carbonyl carbon in the pyrrolidone ring. As the drug content increased, T_1 in the slow motional regime increased, indicating that the mobility of the PVP carbonyl carbon decreased. The T_g values of nifedipine–PVP and phenobarbital–PVP solid dispersions decreased as the drug content increased (Tab. 1), indicating that the molecular mobility of the matrices increased with drug content. These findings suggest that T_1 does not reflect the global motion of the PVP–drug matrix but rather the localized motion of the PVP pyrrolidone ring. The decreased local mobility of the pyrrolidone ring was supported by changes in the T_1 of the C-2 carbon of the pyrrolidone ring. Figure 6 shows the effect of phenobarbital on the T_1 of the C-2 carbon of the pyrrolidone ring. The T_1 value increased in a similar manner to that of the PVP carbonyl carbon shown in Figure 5. The signals of the C-3 and C-α carbons of PVP overlap

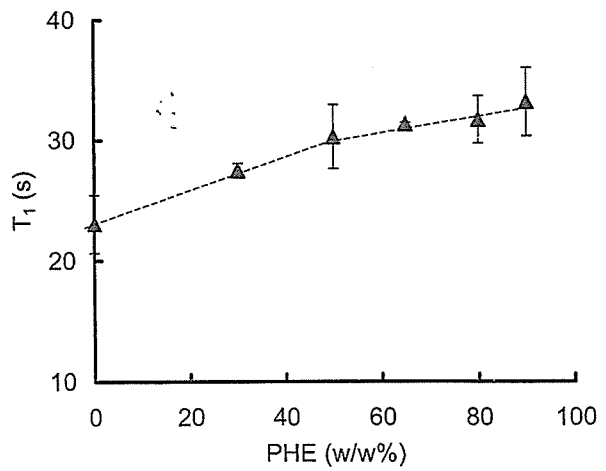

Figure 6. Effect of phenobarbital content on the T_1 of the PVP C-2 carbon in phenobarbital–PVP. Error bars represent standard deviation ($n = 3$).

each other and are observed at 45 ppm. The apparent T_1 of these carbon atoms increased in the presence of nifedipine and phenobarbital in a similar manner to that of the PVP carbonyl carbon (data not shown). Although the C-2 and C-3 carbons are not considered to interact directly with phenobarbital or nifedipine, the interaction of the PVP carbonyl carbon may decrease the motion of all the carbon atoms in the pyrrolidone ring. In summary, hydrogen bond interactions between PVP and the drugs appeared to affect the chemical shift of the PVP carbonyl carbon as well as the T_1 values of the carbonyl, C-2 and C-3 carbons of PVP. Changes in the T_1 value seem to be a more useful measure than chemical shift for detecting PVP–drug interactions, since changes in T_1 were larger than those in chemical shift.

Effect of PVP Content on the T_1 Values of Drug Carbons

Figure 7 shows the effect of PVP content on the T_1 of the phenobarbital C-2, C-4, C-5, and C-6 carbons. The T_1 values of these carbons increased as the PVP content increased. This increase in T_1 became less obvious at PVP contents greater than approximately 35 w/w%, corresponding to a molar ratio of phenobarbital to PVP monomer unit of 1:1. The T_1 values of these carbons increased by 1.5–2 times in the presence of PVP. The order of the relative change in the T_1 values was C-4,6 > C-5>C-2. Although larger change in T_1 values was expected for carbons near the NH group, there was no clear tendency between the relative change in the T_1 values and the proximity of the carbons to the NH group. Hydrogen bond interaction may equally affect the mobility of these carbons, since these carbons comprise the primidinetrione ring. Increased T_1 values after addition of PVP were also observed for nifedipine carbons observed at 103 ppm, as shown in Figure 8. The T_1 values increased as the PVP content increased, in a similar manner to that observed for phenobarbital–PVP solid dispersions. This finding suggests that the localized motion of the drugs decreased as a result of hydrogen bond interactions between PVP and the drugs. This is consistent with the results obtained for PVP carbons described above. PVP affected the T_1 of phenobarbital C-2, C-4, C-5, and C-6 carbons and the T_1 of nifedipine carbons observed at 103 ppm. This may be due to the differences in the interaction site of the drugs; in contrast to nifedipine having one NH group, phenobarbital has two NH groups that can interact with PVP carbonyl. The fact suggests that PVP may decrease the localized motion of phenobarbital more effectively than it does that of nifedipine. The difference in the ability of PVP to decrease the localized motion of the two drugs may explain the difference in the ability of PVP to stabilize amorphous phenobarbital and nifedipine; the overall crystallization rate of amorphous phenobarbital was reduced by 2–3 orders of magnitude by 5 w/w% PVP, whereas 10 w/w% PVP was required to

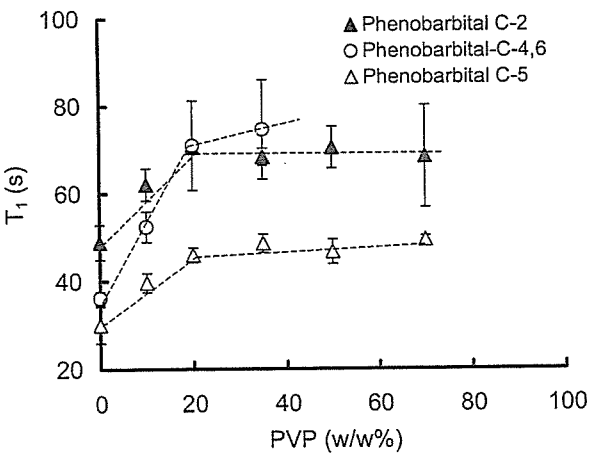

Figure 7. Effect of PVP on the T_1 of phenobarbital carbons. Error bars represent standard deviation ($n = 3$).

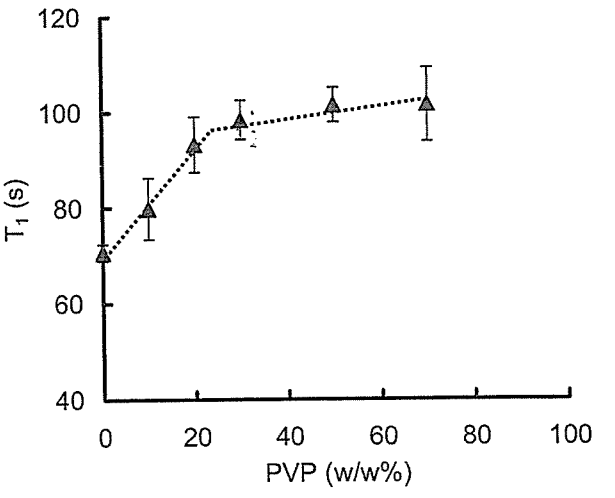

Figure 8. Effect of PVP on the T_1 of nifedipine carbons at 103 ppm (C-2, C-6). Error bars represent standard deviation ($n = 3$).

achieve a similar effect with nifedipine.[10] Therefore, inhibition of the localized motion of drugs appears to be one of the mechanisms by which PVP stabilizes the amorphous state.

CONCLUSION

Changes in the chemical shift of the PVP carbonyl carbon suggest the occurrence of hydrogen bond interactions between the PVP carbonyl group and nifedipine or phenobarbital. These interactions increased the T_1 values of the carbon atoms of PVP and the drugs, suggesting that the localized molecular motion of the drugs was decreased. This decreased molecular mobility appears to be one of the factors that stabilize the amorphous state of drugs.

ACKNOWLEDGMENTS

A part of this work was supported by a Grant-in-aid for Research on Health Sciences Focusing on Drug Innovation from The Japan Health Sciences Foundation.

REFERENCES

1. Yoshioka M, Hancock BC, Zografi G. 1995. Inhibition of indomethacin crystallization in Poly(vinylpyrrolidone) coprecipitate. J Pharm Sci 84:983–986.
2. Matsumoto T, Zografi G. 1999. Physical properties of solid molecular dispersions of indomethacin with poly(vinylpyrrolidone) and poly(vinylpyrrolidone-co-vinyl-acetate) in relation to indomethacin crystallization. Pharm Res 16:1722–1728.
3. Crowley KJ, Zografi G. 2003. The effect of low concentrations of molecularly dispersed poly(vinylpyrrolidone) on indomethacin crystallization from the amorphous state. Pharm Res 20:1417–1422.
4. Shamblin SL, Huang EY, Zografi G. 1996. The effects of co-lyophilized polymer additives on the glass transition temperature and crystallization of amorphous sucrose. J Thermal Anal 47:1567–1579.
5. Shamblin SL, Zografi G. 1999. The effect of absorbed water on the properties of amorphous mixtures containing sucrose. Pharm Res 16:1119–1124.
6. Zeng XM, Martin GP, Marriott C. 2000. Effects of molecular weight of polyvinylpyrrolidone on the glass transition temperature and crystallization of co-lyophilized sucrose. Int J Pharm 218:63–73.
7. Miyazaki T, Yoshioka S, Aso Y, Kojima S. 2004. Ability of polyvinylpyrrolidone and polyacrylic acid to inhibit the crystallization of amorphous acetaminophen. J Pharm Sci 93:2710–2717.
8. Khougaz K, Clas S. 2000. Crystallization inhibition in solid dispersions of MK-0591 and poly(vinylpyrrolidone) polymer. J Pharm Sci 89:1325–1334.
9. Berggren J, Alderborn G. 2004. Long-term stabilization potential of poly(vinylpyrrolidone) for amorphous lactose in spray-dried composites. Eur J Pharm Sci 21:209–215.
10. Aso Y, Yoshioka S, Kojima S. 2004. Molecular mobility-based estimation of the crystallization rates of amorphous nifedipine and phenobarbital in poly(vinylpyrrolidone) solid dispersions. J Pharm Sci 93:384–391.
11. Foster A, Hempennstall J, Rades T. 2001. Characterization of glass solutions of poorly water-soluble drugs produced by melt extrusion with hydrophilic amorpous polymers. J Pharm Pharmacol 53:303–315.
12. Taylor LS, Zografi G. 1997. Spectroscopic characterization of interactions between PVP and indomethacin in amorphous molecular dispersions. Pharm Res 14:1691–1698.
13. Shamblin SS, Taylor LS, Zografi G. 1998. Mixing tendencies of co-lyophilized sucrose-additive systems. J Pharm Sci 87:694–701.
14. Taylor LS, Zografi G. 1998. Sugar-polymer hydrogen bond interactions in lyophilized mixtures. J Pharm Sci 87:1615–1621.
15. Taylor LS, Langkilde FW, Zografi G. 2001. Fourier transform Raman spectroscopic study of the interaction of water vapor with amorphous polymers. J Pharm Sci 90:888–901.
16. Zhang J, Zografi G. 2001. Water vapor absorption into amorphous sucrose-poly (vinylpyrrolidone) and trehalose-poly(vinylpyrrolidone) mixtures. J Pharm Sci 90:1375–1385.
17. Crowly KJ, Zografi G. 2002. Water vapor sorption into amorphous hydrophobic drug/poly(vinylpyrrolidode) dispersions J Pharm Sci 91:2150–2165.
18. Shamblin SL, Zografi G. 1998. Enthalpy relaxation in binary amorphous mixtures containing sucrose. Pharm Res 15:1828–1834.
19. Oksanen CA, Zografi G. 1993. Molecular mobility in mixtures of absorbed water and solid poly(vinylpyrrolidone). Pharm Res 10:791–799.
20. Yoshioka S, Aso Y, Kojima S, Sakurai S, Fujiwara T, Akutsu H. 1999. Molecular mobility of protein lyophilized formulations linked to the molecular mobility of polymer excipients as determined by high resolution ^{13}C solid-state NMR. Pharm Res 16:1621–1625.
21. Aso Y, Sumie Yoshioka S, Zhang J, Zografi G. 2002. Effect of water on the molecular mobility of sucrose and PVP in a colyophilized formulation as measured by ^{13}C–NMR relaxation time. Chem Pharm Bull 50:822–826.

22. Yoshioka S, Aso Y, Kojima S. 2003. Molecular mobility of lyophilized poly(vinylpyrrolidone) and methyl cellulose as determined by the laboratory and rotating frame spin-lattice relaxation time of ^{1}H and ^{13}C. Chem Pharm Bull 51:1289–1292.
23. Yoshie N, Azuma Y, Sakurai M, Inoue Y. 1995. Crystallization and compatibility of poly(vinyl alcohol)/poly(3-hydroxybutyrate) blends: Influence of blend composition and tacticity of poly(vinyl alcohol). J Apply Polym Sci 56:17–24.
24. Kato Y, Watanabe F. 1978. Relationship between polymorphism and bioavailability of phenobarbital. Yakugaku Zasshi 98:639–648.
25. Torchia DA. 1978. The measurement of proton-enhanced carbon–13 T_1 values by a method that suppresses artifacts. J Magn Reson 30:613–618.
26. Yokota K, Abe A, Hosaka S, Sakai I, Saito H. 1978. A ^{13}C nuclear magnetic resonance study of covalently cross-linked gels. Effect of chemical composition, degree of cross-linking, and temperature to chain mobility. Macromolecules 11:95–100.
27. Gaggelli E, Marchettini N, Valensin G. 1987. Nuclear magnetic resonance investigations of calcium-antagonist drugs. Part1. Conformational and dynamic features of nimodipine {3-[(2-methoxyethoxy)carbonyl]-5-(isopropoxycarbonyl)-4-(3-nitrophenyl)-2,6-dimethyl-1,4-dihydropyridine} in [$^{1}H_6$] dimethyl sulphoxide. J Chem Soc Perkin Trans II 1987:1707–1711.
28. Kovesdi I, Kapiller-Dezsofi R. 1996. NMR investigation of nifedipine. Acta Pharm Hung 66:11–14.
29. Soine WH, Soine PJ, England TM, Overton BW, Merat S. 1989. Synthesis of N-β-D-glucopyranosyl derivatives of barbital, phenobarbital, metharbital, and mephobarbital. Carbohydrate Res 19:105–113.
30. Belciug MP, Ananthanarayanan VS. 1994. Interaction of calcium channel antagonists with calcium: Structural studies on nicardipine and its Ca^{2+} complex. J Med Chem 37:4392–4399.

Combination of non-viral connexin 43 gene therapy and docetaxel inhibits the growth of human prostate cancer in mice

MASAYOSHI FUKUSHIMA, YOSHIYUKI HATTORI, TAKASHI YOSHIZAWA and YOSHIE MAITANI

Institute of Medicinal Chemistry, Hoshi University, Shinagawa-ku, Tokyo 142-8501, Japan

Received August 24, 2006; Accepted November 23, 2006

Abstract. Docetaxel (DTX) is used for the treatment of advanced hormone refractory prostate cancer. Connexin 43 (Cx43) is a tumor suppressor gene, and transfection of the Cx43 gene increases sensitivity to several chemotherapeutic agents. The objective of this study was to evaluate the effectiveness of combination therapy of Cx43-expressing plasmid DNA (pCMV-Cx43) and DTX both *in vitro* and *in vivo* using a non-viral vector in human prostate cancer PC-3 cells. Transfection of pCMV-Cx43 into the cells neither inhibited tumor growth nor increased gap junctional intercellular communication; however, combination therapy of pCMV-Cx43 and DTX significantly inhibited cell growth. Forced expression of Cx43 in the cells induced apoptotic cells by down-regulation of Bcl-2 expression and significantly more up-regulation of caspase-3 activity than either treatment alone. The combination of repeated intratumoral injection of pCMV-Cx43 (10 μg/tumor) with non-viral vector and a single intravenous injection of DTX (15 mg/kg) was compared with a repeated injection of Cx43 alone and a single injection of DTX alone on PC-3 tumor xenografts. Significant antitumoral effects were observed in mice receiving combined treatment, compared with DTX alone. The data presented here provide a rational strategy for treating patients with advanced hormone refractory prostate cancer.

Introduction

Prostate cancer is a significant problem and is reported to be the leading cancer diagnosed in man (1). Cytotoxic chemotherapy has shown significant palliative benefit in the treatment of androgen-independent prostate cancer, but with no survival advantage demonstrated to date (2). Current chemotherapy is limited by drug tolerance and the ultimate emergence of resistant disease (3). Novel approaches incorporating potentially more active and less toxic agents that may overcome drug resistance mechanisms need to be investigated. Increased understanding of the tumor biology of prostate cancer offers promise of novel treatments for this disease.

Docetaxel (DTX), a member of the taxane family, is semisynthesized from an inactive taxoid precursor extracted from the needles of the European yew, *Taxus baccata*. DTX has shown clinical activity in a wide spectrum of solid tumors including breast, lung, ovarian, and prostate cancers (4,5). The known basic cellular target of DTX is the microtubule. Furthermore, DTX down-regulates genes for cell proliferation, mitotic spindle formation, transcription factor, and oncogenesis, and up-regulates genes related to the induction of apoptosis and cell cycle arrest in prostate cancer PC-3 and LNCaP cells (6,7).

Connexins (Cxs) are a family of transmembrane proteins that enable gap junctional intercellular communication (GJIC) (8). GJIC is one mechanism of growth control that involves cell-cell contact (9). In general, cancer cells exhibit altered Cxs expression, with a profile that is often significantly reduced or undetectable. Connexin 43 (Cx43) and connexin 32 (Cx32) expressions were reduced in prostate tumor biopsy in contrast to normal prostate epithelial cells (10-13). Since Cx43 is a tumor-suppressor gene, Cx43 gene therapy was reported (14-16). Transfection of Cx43 in human mammary carcinoma MDA-MB-435 cells (17), human glioblastoma U251 and T98G cells (16), lung cancer PG cells (18) and prostate cancer LNCaP cells (19) significantly reduces cell growth *in vitro* and/or *in vivo*. Transfection of Cx43 in human glioblastoma U251 cells (20) and ovarian carcinoma SKOV-3 cells (21) increased sensitivity to several chemotherapeutic agents. However, the effect of transfection of the Cx gene combined with DTX on prostate tumor PC-3 cells has not been reported to our knowledge.

In this study, we investigated whether the transfection of plasmid DNA (pCMV-Cx43) coding for the Cx43 gene by non-viral vector combined with DTX increased the inhibition of PC-3 cell growth. A novel combination of pCMV-Cx43 and DTX induced significantly greater growth inhibition in PC-3 cells and tumor xenografts than DTX alone. This combination increased apoptosis via the down-regulation of Bcl-2 expression and up-regulation of caspase-3 activity.

Materials and methods

Cell culture. PC-3 and LNCaP cells were supplied by the Cell Resource Center for Biomedical Research, Tohoku University.

Correspondence to: Professor Yoshie Maitani, Institute of Medicinal Chemistry, Hoshi University, Shinagawa-ku, Tokyo 142-8501, Japan
E-mail: yoshie@hoshi.ac.jp

Key words: prostate cancer, connexin 43, docetaxel, PC-3 cells, cytotoxicity, gene therapy, non-viral vector, combination therapy

PC-3 and LNCaP cells were grown in RPMI-1640 medium supplemented with 10% heat-inactivated fetal bovine serum (FBS) and kanamycin (100 μg/ml) at 37˚C in a 5% CO_2 humidified atmosphere.

Plasmid constructions. Plasmid pCMV-Cx43 encoding the Cx43 gene under the control of CMV promoter was constructed as previously described (22). Plasmid pCMV-luc encoding the luciferase gene under the control of the CMV promoter was constructed as previously described (23). pGL3-basic (Promega, Madison, WI) was used as a control plasmid. A protein-free preparation of the plasmid was purified following alkaline lysis using maxiprep columns (Qiagen, Hilden, Germany).

Sensitivity to DTX assay. PC-3 and LNCaP cells were seeded separately at a density of $1x10^4$ cells per well in 96-well plates and maintained for 24 h before transfection in RPMI medium supplemented with 10% FBS. Cells at 30% confluence in the well were transfected with 0.2 μg of pCMV-Cx43 or pGL3-basic using lipofectamine 2000 (Invitrogen Corp., Carlsbad, CA) according to the manufacturer's instructions and incubated for 24 h. The culture medium was then exchanged to medium containing various concentrations of DTX (Taxotere, Sanofi-Aventis, Paris, France) ranging from 0.1 to 1,000 ng/ml and incubated for another 48 h. In co-transfection, cells were transfected with 0.2 μg of pCMV-Cx43 or pGL3-basic using lipofectamine 2000 in medium containing DTX (0.1-1,000 ng/ml) and incubated for 72 h. The cell number was determined with WST-8 assay (Dojindo Laboratories, Kumamoto, Japan).

Fluorescent dye transfer. FACS analysis of the GJIC reported by Robe *et al* (24) was modified. Briefly, cells grown in 35-mm dishes were labeled for 1-h incubation with either 5 μM calcein-AM (acetomethylic ester, Dojindo) or 5 μM DiI (Lambda Probes & Diagnostics, Graz, Austria) in the medium. The two labeled cells were mixed in equal proportions in 35-mm dishes and incubated for 12 h. Subsequently, pCMV-Cx43 or pGL3-basic was transfected into mixed cells in the presence or absence of 50 μM 18α-glycyrrhethinic acid (18GA, MP Biomedicals, Germany). After 24-h incubation, the cells were trypsinized, washed in phosphate-buffered saline pH 7.4 (PBS), and processed for FACS analysis of calcein-AM and DiI fluorescence with a FACSCalibur flow cytometer as previously reported (22). Data for 10,000 fluorescent events were obtained by calcein-AM fluorescence (530/30 nm) and DiI fluorescence (585/42).

Cell cycle analysis. PC-3 cells were seeded at a density of $1x10^6$ cells on 35-mm dishes. Cells were transfected with pCMV-Cx43 or pGL3-basic in the presence or absence of 10 ng/ml DTX in medium. After 24-h incubation, the cells were harvested with EDTA after washing with ice-cold PBS. Detached cells were washed once with ice-cold PBS and gently suspended in PBS-EtOH (70%) and fixed overnight at 4˚C. For staining, fixed cells were washed once in PBS and then resuspended in PBS with 50 μg/ml propidium iodide (PI) and 0.5% RNase A. After 30 min at 37˚C, cells were processed for FACS analysis of PI fluorescence by a FACSCalibur flow cytometer as described in the above section.

Western blotting. PC-3 cells were seeded at a density of $1x10^6$ cells on 35-mm dishes. Cells were transfected with pGL3-basic or pCMV-Cx43, respectively. Twenty-four hours after transfection, the culture medium was replaced with medium containing 10 ng/ml DTX and incubated for 24 h. Cells were suspended in lysis buffer (1% Triton-X 100 and protease inhibitor cocktail set III (Calbiochem, Darmstadt, Germany) in PBS), and then centrifuged at 15,000 rpm for 10 min. The supernatants were resolved on a 15% sodium dodecyl sulphate-polyacrylamide gel by electrophoresis (SDS-PAGE) and transferred to a polyvinylidene difluoride (PVDF) membrane (FluoroTrans® W, PALL Gelman Laboratory, Ann Arbor, MI). Expression of Cx43, Bcl-2 and ß-actin protein was identified using rabbit anti-Cx43 polyclonal antibody (Sigma, St. Louis, MO), rabbit anti-Bcl-2 polyclonal antibody (Stressgen, Canada) or rabbit anti-ß-actin polyclonal antibody (Lab Vision, CA), respectively. Goat anti-rabbit IgG peroxidase conjugate (Santa Cruz Biotechnology, Inc., Santa Cruz, CA) was used as the secondary antibody. These proteins were detected with peroxidase-induced chemiluminescence (Super Signal West Pico Chemiluminescent Substrate, Pierce). Optical density of the bands on the film was quantified using ImageQuant TL (Amersham Biosciences, NJ) with correction for the optical density of the corresponding ß-actin band.

Apoptosis analysis. PC-3 cells were seeded at a density of $1x10^6$ cells on 35-mm dishes. The cells were transfected with pGL3-basic or pCMV-Cx43, respectively. Twenty-four hours after transfection, the culture medium was replaced with medium containing 10 ng/ml DTX and incubated for 24 h. Apoptotic cells were detected with an annexin V-FITC apoptosis detection kit (Sigma) or caspase-3 apoptosis detection kit (Santa Cruz Biotechnology) according to the manufacturer's instructions.

Assessment of PC-3 tumor growth. For transfection *in vivo*, we prepared cationic nanoparticle (NP) as previously reported (25). Briefly, NP was formulated using 1 mg/ml cholesteryl-3ß-carboxyamidoethylene-*N*-hydroxyethylamine (OH-Chol) as a cationic lipid, and 5 mol% Tween-80, and was prepared in 10 ml of water by the modified ethanol injection method (25).

Male BALB/c nu/nu mice (6-8 weeks of age) were purchased from CLEA Japan Inc. (Tokyo, Japan). To generate PC-3 tumor xenografts, $1x10^7$ PC-3 cells suspended in 50 ml of medium containing 60% reconstituted basement membrane (Matrigel: Collaborative Research, Bedford, MA) were inoculated subcutaneously into the flank region of the mice. Tumor volume was calculated using the formula, tumor volume $= 0.5ab^2$, where a and b are the larger and smaller diameters, respectively. When the average volume of PC-3 xenograft tumors reached 200 mm^3 (day 0), these mice were selected for treatment with DTX alone, pGL3-basic, pCMV-Cx43, pGL3-basic plus DTX, and pCMV-Cx43 plus DTX. For transfection into tumors, the nanoplex was formed by the addition of NP (15.8 μl) to 10 μg of pCMV-Cx43 or pGL3-basic with gentle shaking and standing at room temperature for 10 min. Nanoplexes of 10 μg plasmid per tumor were directly injected into xenografts on days 0 and 1. DTX at a dose of 15 mg/kg was injected i.v. on day 0. Tumor volume was measured on days 0, 3, 6, 9, 11, 13, 15. On day 15, all

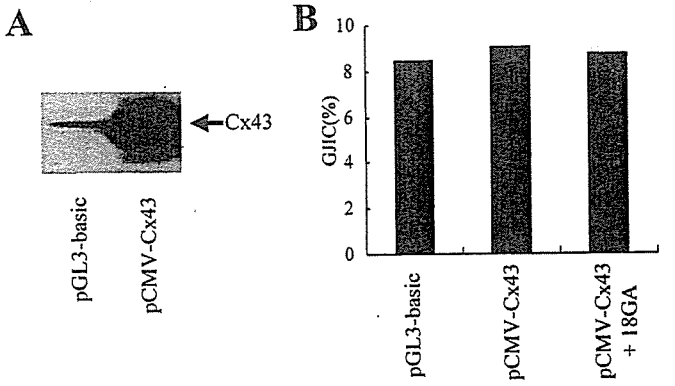

Figure 1. Cx43 expression and GJIC transfected with pCMV-Cx43 in PC-3 cells. (A) Western blot analyses of Cx43 in the cells 24 h after transfection with pCMV-Cx43 or pGL3-basic. (B) Effect of Cx43 transfection on gap junctional intercellular communication (GJIC) analyzed by flow cytometry. Calcein-AM-labeled cells were mixed with DiI-labeled cells, and transfected with pCMV-Cx43 or pGL3-basic. Cells were incubated for 24 h in the presence or absence of 50 μM 18GA.

mice were sacrificed after anesthetization by i.m. injection of pentobarbital (Nembutal, Dainippon Pharmaceutical Co., Ltd., Osaka, Japan), and the tumor weights were measured. The data are shown as the mean ± SE. Animal experiments were conducted with ethical approval from our institutional animal care and use committee.

Statistical analysis. The statistical significance of the data was evaluated with Student's t-test. A $P \leq 0.05$ was considered significant.

Results

Effect of Cx43 expression on PC-3 cells. We initially characterized the expression of Cx43 in PC-3 cells. In this study, we used pGL3-basic as a control plasmid. Cx43 expression was observed strongly in pCMV-Cx43-transfected cells, but weakly in pGL3-basic-transfected cells (Fig. 1A). Next, we examined whether the transfection of pCMV-Cx43 induced growth inhibition in the cells. Seventy-two hours after transfection, Cx43 expression did not significantly induce a suppressive effect in PC-3 cells (data not shown).

To investigate whether the expression of Cx43 protein by pCMV-Cx43 caused the formation of gap junctions, we assessed the transfer of calcein-AM, a cytoplasmic dye that crosses gap junctions, in co-culture with calcein-AM-loaded cells and cells marked with DiI, a non-diffusible membrane fluorescent dye, by FACS analysis. As shown in Fig. 1B, GJIC (%) was not significantly increased in pCMV-Cx43-transfected cells compared with pGL3-basic-transfected cells. Moreover, pCMV-Cx43-transfected cells treated with 18GA, GJIC inhibitor did not decrease either the GJIC (%) compared with pGL3-basic- or pCMV-Cx43-transfected cells (Fig. 1B).

In vitro sensitivity of DTX. To evaluate the *in vitro* growth inhibitory effect of combination therapy of Cx43 and DTX, the WST-8 assay was initially performed. When PC-3 cells were transfected with pGL3-basic or pCMV-Cx43 in the presence of DTX, pCMV-Cx43-transfected cells (IC_{50} = 1.1 ng/ml) showed 53-fold higher sensitivity to DTX than pGL3-basic-transfected cells (IC_{50} = 58.7 ng/ml) (Fig. 2A). However, when PC-3 cells were treated with DTX 24 h after the transfection of pGL3-basic or pCMV-Cx43, pCMV-Cx43-transfected cells (IC_{50} = 1.4 ng/ml) showed 279-fold higher sensitivity to DTX than pGL3-basic-transfected cells (IC_{50} = 390.0 ng/ml) (Fig. 2B). When PC-3 cells were transfected with pCMV-Cx43 24 h after treatment with DTX, cytotoxicity could not be evaluated since cells were almost dead even at 1 ng/ml of DTX (data not shown). Therefore, in subsequent *in vitro* experiments, the cells were treated with DTX 24 h after transfection of pCMV-Cx43.

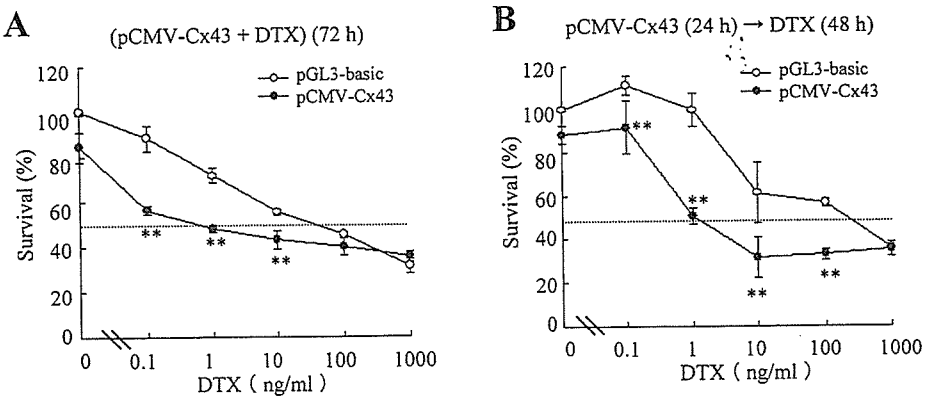

	IC_{50} (ng/ml)	(%)
pGL3-basic	58.7	100.0
pCMV-Cx43	1.1	1.8

	IC_{50} (ng/ml)	(%)
pGL3-basic	390.0	100.0
pCMV-Cx43	1.4	0.4

Figure 2. Concentration-dependent effect of DTX on cytotoxicity in Cx43-transfected cells. (A) Cells were transfected with 0.2 μg of pCMV-Cx43 or pGL3-basic in the presence of DTX and incubated for 72 h. (B) PC-3 cells were transfected with pCMV-Cx43 or pGL3-basic for 24 h. After incubation, cells were treated with various concentrations of DTX and incubated for another 48 h. The number of viable cells was determined by WST-8 assay. n=3 for each sample. **$p<0.01$; compared with pGL3-basic.

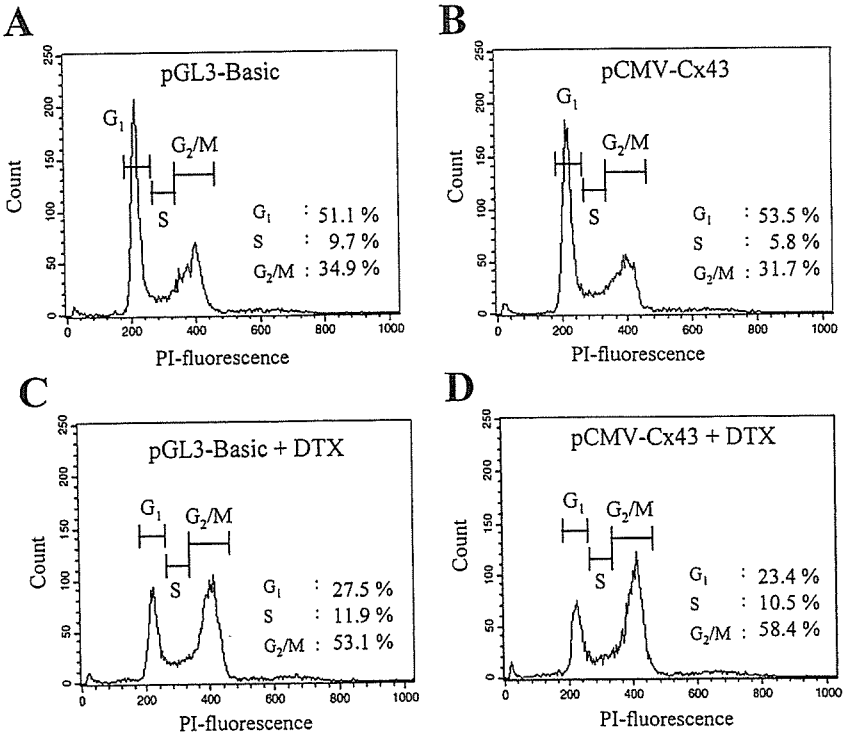

Figure 3. Cell cycle kinetics of pGL3-basic (A), pCMV-Cx43 (B), pGL3-basic plus 10 ng/ml DTX (C), and pCMV-Cx43 plus 10 ng/ml DTX (D) 24 h after transfection into PC-3 cells. Histograms illustrate the differences in G_1, S, and G_2/M phases upon transfection into PC-3 cells.

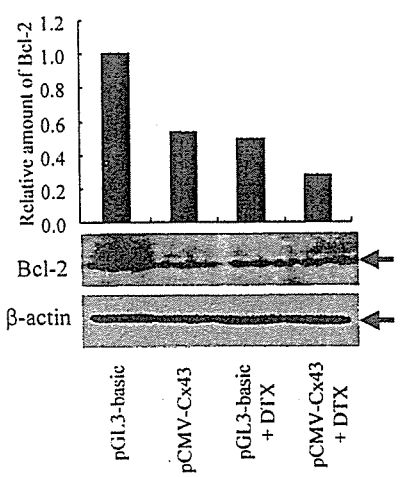

Figure 4. Decrease of Bcl-2 expression in PC-3 cells by combination therapy of Cx43 and DTX. Cells were transfected with pGL3-basic or pCMV-Cx43 for 24 h. Culture medium was replaced with medium containing of 10 ng/ml DTX and incubated for another 24 h. Bcl-2 expression was examined by Western blot analyses, quantified using densitometry.

We next assessed the effect of pCMV-Cx43 and DTX on the cell cycle 24 h after transfection into PC-3 cells by flow cytometric analysis. Transfection of pCMV-Cx43 into the cells did not affect the cell cycle (Fig. 3A and B), but DTX caused an increase in G_2/M populations (53.1%) (Fig. 3C). Co-transfection of pCMV-Cx43 with DTX resulted in substantial accumulation in G_2 (58.4%) populations (Fig. 3D).

Effect of Bcl-2 expression and apoptosis activity on PC-3 cells. Recently, it has been reported that transfection of Cx down-regulated the levels of Bcl-2 (20,26,27). Therefore, to investigate whether transfection with pCMV-Cx43 and/or treatment with DTX affected Bcl-2 expression in PC-3 cells, we examined the levels of protein expression of Bcl-2 in the cells by Western blotting. Either pCMV-Cx43-transfection or DTX treatment down-regulated the levels of Bcl-2 (Fig. 4). Moreover, pCMV-Cx43-transfected cells treated with DTX exhibited the most down-regulated level of Bcl-2 compared with pGL3-basic-transfected cells (Fig. 4).

Next, we examined the apoptotic effect in cells transfected with Cx43 and/or treated with DTX by annexin V assay. As shown in Fig. 5A, pCMV-Cx43 transfection or treatment with DTX increased apoptosis in the cells compared with pGL3-basic transfection. Moreover, the incidence of apoptosis was highest in pCMV-Cx43-transfected cells treated with DTX.

To investigate the apoptosis mechanism by combination therapy of Cx43 and DTX, we measured caspase-3 activity. As shown in Fig. 5B, caspase-3 activity in pCMV-Cx43-transfected cells, pGL3-basic-transfected cells with DTX and pCMV-Cx43-transfected cells with DTX was 1.6-, 1.4- and 2.0-fold higher than that in pGL3-basic-transfected cells, respectively. Forced expression of Cx43 in the cells induced significantly more up-regulation of caspase-3 activity than either treatment alone. These results suggest that the constitutive expression of Cx43 may play a role in the enhancement of apoptosis by chemotherapeutic agents.

Synergistic inhibition of the growth of PC-3 tumor xenografts. The efficacy of combination therapy of Cx43 and DTX in inhibiting the growth of subcutaneous PC-3 tumors was evaluated. We previously reported that NP could efficiently

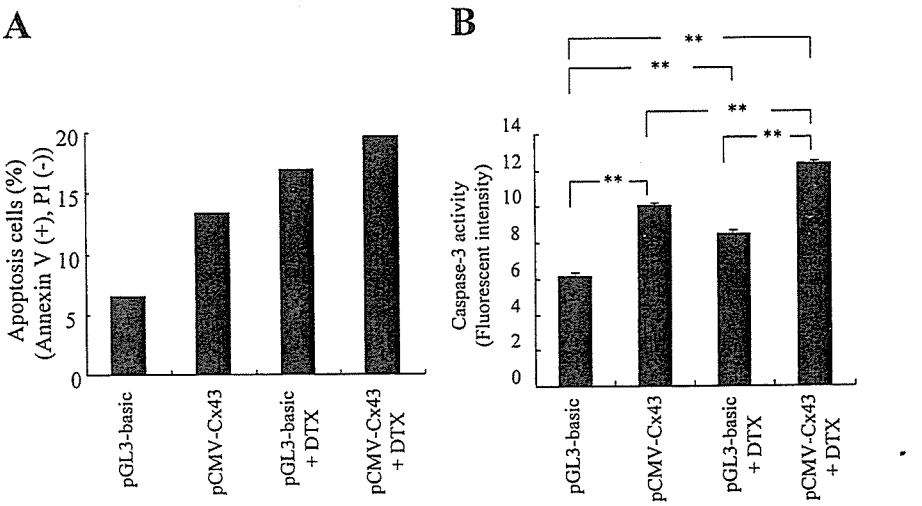

Figure 5. Apoptotic cells and caspase-3 activity by combined treatment with Cx43 and DTX on PC-3 cells. Cells were transfected with pGL3-basic or pCMV-Cx43 and incubated for 24 h. Culture medium was replaced with medium containing 10 ng/ml DTX, and incubated for another 24 h. Apoptotic cells and caspase-3 activity were detected by annexin V assay (A) and caspase-3 fluorometric assay (B). (B), n=3 for each sample. **p<0.01.

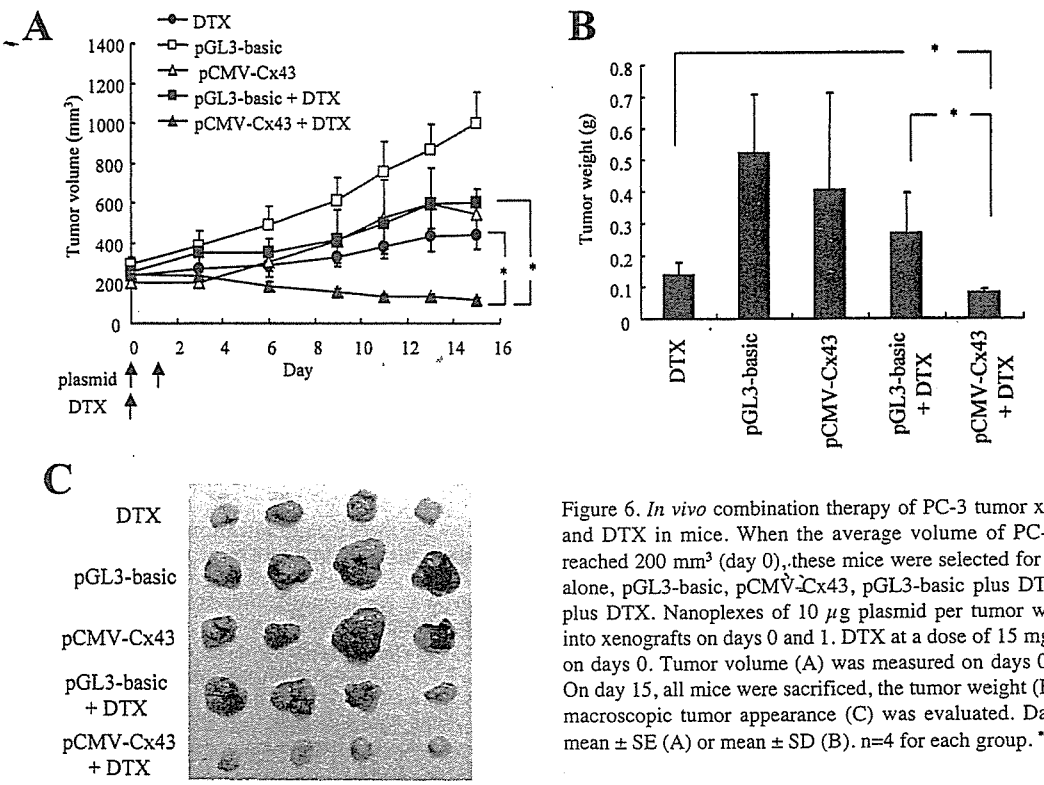

Figure 6. *In vivo* combination therapy of PC-3 tumor xenografts with Cx43 and DTX in mice. When the average volume of PC-3 xenograft tumors reached 200 mm³ (day 0), these mice were selected for treatment with DTX alone, pGL3-basic, pCMV-Cx43, pGL3-basic plus DTX and pCMV-Cx43 plus DTX. Nanoplexes of 10 μg plasmid per tumor were directly injected into xenografts on days 0 and 1. DTX at a dose of 15 mg/kg was injected i.v. on days 0. Tumor volume (A) was measured on days 0, 3, 6, 9, 11, 13, 15. On day 15, all mice were sacrificed, the tumor weight (B) was measured and macroscopic tumor appearance (C) was evaluated. Data are shown as the mean ± SE (A) or mean ± SD (B). n=4 for each group. *p<0.05.

deliver DNA into PC-3 xenografts (28). Therefore, we used NP as a DNA transfection vector for *in vivo* experiment. The anti-tumor effect was evaluated by direct injection of the nanoplex of pCMV-Cx43 or pGL3-basic into the xenografts once a day on two occasions (day 0 and 1) following one i.v. injection of DTX (day 0) according to a previous report on *in vivo* combination gene therapy with DTX (29). No significant decrease in tumor weight was observed in mice treated with pCMV-Cx43 (Fig. 6B). A growth inhibitory effect was observed in mice treated with DTX alone or pGL3-basic plus DTX compared with control mice (Fig. 6A and B). pGL3-basic plus DTX exhibited a similar tumor suppressive effect with DTX alone, indicating that DNA transfection did not increase tumor growth inhibition. A significant growth inhibitory effect was observed in combination therapy of pCMV-Cx43 and DTX compared with DTX alone (Fig. 6A and B). A comparison of tumor weight and the appearance after excision also demonstrated that tumor growth was attenuated in mice treated with pCMV-Cx43 and DTX (Fig. 6B and C).

Discussion

The limited efficacy of cytotoxic chemotherapy remains a major problem in the treatment of advanced hormone-refractory prostate cancer (30); therefore, novel cancer gene therapy needs to be developed. In this study, we found that Cx43 expression in PC-3 cells significantly enhanced DTX cytotoxicity through down-regulation of Bcl-2 expression and activation of the apoptosis pathway. Furthermore, the combination of non-viral Cx43 gene therapy and DTX significantly suppressed the growth of tumor xenografts compared to DTX alone. This is the first report to highlight that the expression of Cx43 in association with DTX has potential as a tumor growth inhibitor.

Dysregulation of Cx expression is thought to be associated with carcinogenesis; however, there is relatively little information regarding the mechanism of altered Cx expression in prostate cancer. The tumor-suppressing effects of Cx genes largely depend on the Cx species and the cell types used (31). Transduction of Cx32 and Cx43 by retroviral gene transfection into the Cx-deficient prostate cancer cell line LNCaP produced growth inhibition *in vitro* and *in vivo*, and cell differentiation associated with gap junction formation (19). Transduction of Cx26 by adenoviral gene transfection into LNCaP and PC-3 cells produced growth inhibition by a GJIC function (26). Regarding Cx43, the expression of Cx43 in PC-3 cells could not form gap junctions (32). In our study, the transfection of pCMV-Cx43 into PC-3 cells exhibited neither the inhibition of cell growth nor increased GJIC (Fig. 1); however, transfection into the cells increased apoptotic cells and caspase-3 activity (Fig. 5). Cx43 expression in PC-3 cells might regulate apoptosis via a GJIC-independent mechanism.

Combination therapy of Cx43 and DTX was significantly more cytotoxic when cells were treated with DTX 24 h after Cx43 transfection compared with treatment with DTX and transfection at the same time. It suggested that Cx43 expression 24 h after transfection affected sensitivity to DTX. We also found that combination therapy 72 h after transfection increased growth inhibition in LNCaP cells (IC_{50} for DTX = 32 and 4.2 ng/ml in pGL3-basic- and pCMV-Cx43-transfected cells, respectively) (data not shown). Combination therapy using the Cx gene and chemotherapeutic agents for cancer has been reported. Cx43 transfected into human glioblastoma cells (20) and ovarian carcinoma cells (21) led to the down-regulation of Bcl-2 and increased sensitivity to paclitaxel and doxorubicin. In our study, DTX treatment caused an increase in G_2/M populations into PC-3 cells (Fig. 3C), and also induced the down-regulation of Bcl-2 expression and up-regulation of caspase-3 activity in PC-3 cells (Figs. 4 and 5). This finding corresponds with previous reports that DTX induced the down-regulation of Bcl-2 expression in prostate tumor LNCaP and PC-3 cells (33,34), and that down-regulation of Bcl-2 expression by Bcl-2 antisense activated caspase-3 activity in PC-3 cells (35). Combination therapy of pCMV-Cx43 and DTX increased G_2/M populations, enhancing down-regulation of Bcl-2, and growth inhibition *in vitro* more than DTX alone.

The combination of repeated intratumoral injections of pCMV-Cx43 (10 μg/tumor) with non-viral vector and a single intravenous injection of DTX (15 mg/kg) was compared with a repeated injection of Cx43 alone and a single injection of DTX alone in PC-3 tumor xenografts. Significant antitumoral effects were observed in mice receiving combined treatment, compared with DTX alone. The efficacy *in vivo* might result from direct effects of Cx43 on inducing apoptosis and indirect effects on enhancing the cytotoxicity of DTX by down-regulating Bcl-2. It has been reported that paclitaxel increased the transfection efficiency of cationic liposome by inhibiting targeting endosomes to lysosomes (36,37). Therefore, using the combined lipid-mediated transfection of genes with DTX for cancer gene therapy might be a powerful technique due to the effect of enhanced gene expression. Inhibiting Bcl-2 expression by Cx43 in prostate cancer cells, which could restore their sensitivity to chemotherapeutic agents, would be a new therapeutic strategy against prostate cancer.

From a clinical point of view, the doses of DTX used in the combined strategy will be minimal, and will prevent significant toxicity due to DTX. Low doses of DTX can thus be administered in humans for a prolonged period of time, or alternatively, a shorter duration of combined treatment may be administered without loss of effectiveness. Enforced expression of Cx43 increased sensitivity for DTX via the down-regulation of Bcl-2 expression in PC-3 cells. Combining non-viral Cx43 gene therapy with DTX resulted in greater growth suppression of PC-3 *in vitro* and *in vivo*. The data presented here provide a rational strategy for treating patients with advanced hormone refractory prostate cancer.

Acknowledgements

This project was supported in part by a grant from The Promotion and Mutual Aid Corporation for Private Schools of Japan, and by a Grant-in-aid for Scientific Research from the Ministry of Education, Culture, Sports, Science, and Technology of Japan.

References

1. Gao X, Porter AT, Grignon DJ, Pontes JE and Honn KV: Diagnostic and prognostic markers for human prostate cancer. Prostate 31: 264-281, 1997.
2. Oh WK and Kantoff PW: Management of hormone refractory prostate cancer: current standards and future prospects. J Urol 160: 1220-1229, 1998.
3. Syed S: Combination chemotherapy for hormone-refractory prostate carcinoma: progress and pitfalls. Cancer 98: 2088-2090, 2003.
4. Beer TM, El Geneidi M and Eilers KM: Docetaxel (taxotere) in the treatment of prostate cancer. Expert Rev Anticancer Ther 3: 261-268, 2003.
5. Hong WK: The current status of docetaxel in solid tumors. An M.D. Anderson Cancer Center Review. Oncology 16: 9-15, 2002.
6. Pienta KJ: Preclinical mechanisms of action of docetaxel and docetaxel combinations in prostate cancer. Semin Oncol 28: 3-7, 2001.
7. Li Y, Li X, Hussain M and Sarkar FH: Regulation of microtubule, apoptosis, and cell cycle-related genes by taxotere in prostate cancer cells analyzed by microarray. Neoplasia 6: 158-167, 2004.
8. Knuechel R, Siebert-Wellnhofer A, Traub O and Dermietzel R: Connexin expression and intercellular communication in two- and three-dimensional *in vitro* cultures of human bladder carcinoma. Am J Pathol 149: 1321-1332, 1996.
9. Bruzzone R, White TW and Paul DL: Connections with connexins: the molecular basis of direct intercellular signaling. Eur J Biochem 238: 1-27, 1996.

10. Tsai H, Werber J, Davia MO, *et al*: Reduced connexin 43 expression in high grade, human prostatic adenocarcinoma cells. Biochem Biophys Res Commun 227: 64-69, 1996.
11. Hossain MZ, Jagdale AB, Ao P, LeCiel C, Huang RP and Boynton AL: Impaired expression and posttranslational processing of connexin43 and downregulation of gap junctional communication in neoplastic human prostate cells. Prostate 38: 55-59, 1999.
12. Habermann H, Ray V, Habermann W and Prins GS: Alterations in gap junction protein expression in human benign prostatic hyperplasia and prostate cancer. J Urol 167: 655-660, 2002.
13. Mehta PP, Lokeshwar BL, Schiller PC, Bendix MV, Ostenson RC, Howard GA and Roos BA: Gap-junctional communication in normal and neoplastic prostate epithelial cells and its regulation by cAMP. Mol Carcinog 15: 18-32, 1996.
14. Yamasaki H: Role of disrupted gap junctional intercellular communication in detection and characterization of carcinogens. Mutat Res 365: 91-105, 1996.
15. Chen SC, Pelletier DB, Ao P and Boynton AL: Connexin43 reverses the phenotype of transformed cells and alters their expression of cyclin/cyclin-dependent kinases. Cell Growth Differ 6: 681-690, 1995.
16. Huang RP, Fan Y, Hossain MZ, Peng A, Zeng ZL and Boynton AL: Reversion of the neoplastic phenotype of human glioblastoma cells by connexin 43 (cx43). Cancer Res 58: 5089-5096, 1998.
17. Hirschi KK, Xu CE, Tsukamoto T and Sager R: Gap junction genes Cx26 and Cx43 individually suppress the cancer phenotype of human mammary carcinoma cells and restore differentiation potential. Cell Growth Differ 7: 861-870, 1996.
18. Zhang ZQ, Zhang W, Wang NQ, Bani-Yaghoub M, Lin ZX and Naus CC: Suppression of tumorigenicity of human lung carcinoma cells after transfection with connexin43. Carcinogenesis 19: 1889-1894, 1998.
19. Mehta PP, Perez-Stable C, Nadji M, Mian M, Asotra K and Roos BA: Suppression of human prostate cancer cell growth by forced expression of connexin genes. Dev Genet 24: 91-110, 1999.
20. Huang RP, Hossain MZ, Huang R, Gano J, Fan Y and Boynton AL: Connexin 43 (cx43) enhances chemotherapy-induced apoptosis in human glioblastoma cells. Int J Cancer 92: 130-138, 2001.
21. Fernstrom MJ, Koffler LD, Abou-Rjaily G, Boucher PD, Shewach DS and Ruch RJ: Neoplastic reversal of human ovarian carcinoma cells transfected with connexin 43. Exp Mol Pathol 73: 54-60, 2002.
22. Hattori Y and Maitani Y: Folate-linked nanoparticle-mediated suicide gene therapy in human prostate cancer and nasopharyngeal cancer with herpes simplex virus thymidine kinase. Cancer Gene Ther 12: 796-809, 2005.
23. Igarashi S, Hattori Y and Maitani Y: Biosurfactant MEL-A enhances cellular association and gene transfection by cationic liposome. J Control Release 112: 362-368, 2006.
24. Robe PA, Jolois O, N'Guyen M, Princen F, Malgrange B, Merville MP and Bours V: Modulation of the HSV-TK/ganciclovir bystander effect by n-butyrate in glioblastoma: correlation with gap-junction intercellular communication. Int J Oncol 25: 187-192, 2004.
25. Hattori Y, Kubo H, Higashiyama K and Maitani Y: Folate-linked nanoparticles formed with DNA complexes in sodium chloride solution enhance transfection efficiency. J Biomed Nanotech 1: 176-184, 2005.
26. Tanaka M and Grossman HB: Connexin 26 induces growth suppression, apoptosis and increased efficacy of doxorubicin in prostate cancer cells. Oncol Rep 11: 537-541, 2004.
27. Fujimoto E, Sato H, Nagashima Y, *et al*: A Src family inhibitor (PP1) potentiates tumor-suppressive effect of connexin 32 gene in renal cancer cells. Life Sci 76: 2711-2720, 2005.
28. Hattori Y and Maitani Y: Two-step transcriptional amplification-lipid-based nanoparticles using PSMA or midkine promoter for suicide gene therapy in prostate cancer. Cancer Sci 97: 787-798, 2006.
29. Hayashi N, Asano K, Suzuki H, Yamamoto T, Tanigawa N, Egawa S and Manome Y: Adenoviral infection of survivin antisense sensitizes prostate cancer cells to etoposide *in vivo*. Prostate 65: 10-19, 2005.
30. Kasamon KM and Dawson NA: Update on hormone-refractory prostate cancer. Curr Opin Urol 14: 185-193, 2004.
31. Mesnil M, Krutovskikh V, Piccoli C, Elfgang C, Traub O, Willecke K and Yamasaki H: Negative growth control of HeLa cells by connexin genes: connexin species specificity. Cancer Res 55: 629-639, 1995.
32. Govindarajan R, Zhao S, Song XH, Guo RJ, Wheelock M, Johnson KR and Mehta PP: Impaired trafficking of connexins in androgen-independent human prostate cancer cell lines and its mitigation by alpha-catenin. J Biol Chem 277: 50087-50097, 2002.
33. Tang Y, Khan MA, Goloubeva O, Lee DI, Jelovac D, Brodie AM and Hussain A: Docetaxel followed by castration improves outcomes in LNCaP prostate cancer-bearing severe combined immunodeficient mice. Clin Cancer Res 12: 169-174, 2006.
34. Muramaki M, Miyake H, Hara I and Kamidono S: Synergistic inhibition of tumor growth and metastasis by combined treatment with TNP-470 and docetaxel in a human prostate cancer PC-3 model. Int J Oncol 26: 623-628, 2005.
35. Yamanaka K, Rocchi P, Miyake H, Fazli L, Vessella B, Zangemeister-Wittke U and Gleave ME: A novel antisense oligonucleotide inhibiting several antiapoptotic Bcl-2 family members induces apoptosis and enhances chemosensitivity in androgen-independent human prostate cancer PC3 cells. Mol Cancer Ther 4: 1689-1698, 2005.
36. Hasegawa S, Hirashima N and Nakanishi M: Microtubule involvement in the intracellular dynamics for gene transfection mediated by cationic liposomes. Gene Ther 8: 1669-1673, 2001.
37. Nair RR, Rodgers JR and Schwarz LA: Enhancement of transgene expression by combining glucocorticoids and anti-mitotic agents during transient transfection using DNA-cationic liposomes. Mol Ther 5: 455-462, 2002.

Available online at www.sciencedirect.com
SCIENCE DIRECT
ELSEVIER
International Journal of Pharmaceutics 308 (2006) 183–189
INTERNATIONAL JOURNAL OF PHARMACEUTICS
www.elsevier.com/locate/ijpharm

Pharmaceutical Nanotechnology

Preparation of camptothecin-loaded polymeric micelles and evaluation of their incorporation and circulation stability

Masato Watanabe [a], Kumi Kawano [a], Masayuki Yokoyama [b], Praneet Opanasopit [c], Teruo Okano [c], Yoshie Maitani [a,*]

[a] *Institute of Medicinal Chemistry, Hoshi University, Ebara 2-4-41, Shinagawa-ku, Tokyo 142-8501, Japan*
[b] *Kanagawa Academy of Science and Technology, KSP Bldg. East 404, Sakado 3-2-1, Takatu-ku, Kawasaki-shi, Kanagawa-ken, 213-0012, Japan*
[c] *Institute of Advanced Biomedical Engineering and Science, Tokyo Women's Medical University, Kawada-cho 8-1, Shinjuku-ku, Tokyo 162-8666, Japan*

Received 7 July 2005; received in revised form 7 October 2005; accepted 24 October 2005
Available online 29 November 2005

Abstract

To improve its aqueous solubility and stability in biological fluid, CPT was physically loaded in polymeric micelles. Polymeric micelles were composed of various poly(ethylene glycol)–poly(aspartate ester) block copolymers (PEG-P(Asp(R))). The incorporation and circulation stability of CPT micelles were evaluated by measuring the CPT in micelle using gel-permeation chromatography and by CPT concentration measurement after intravenous injection using HPLC, respectively, in terms of chemical structure of block copolymers. The stability of CPT-loaded micelles in vivo depended on the amount of benzyl esters, and length of PEG in the polymers to a greater degree than it did in vitro. A stable formulation of CPT-loaded micelles was obtained using PEG-P(Asp) with PEG of 5000 (MW), 27 Asp units, and 57–75% benzyl esterification of Asp residue. This CPT-loaded micelles showed about a 17-fold lower blood clearance value than unstable micelles. The CPT-loaded micelles are potentially delivered to tumor sites owing to an extended circulation in the blood stream.
© 2005 Elsevier B.V. All rights reserved.

Keywords: Camptothecin; Polymeric micelles; Long circulating; In vivo stability

1. Introduction

Camptothecin (CPT) is a naturally occurring cytotoxic alkaloid isolated from the Chinese plant *Camptotheca accuminata* (Wall et al., 1966). CPT and some of its analogs have shown a broad spectrum of antitumor activity against many solid tumors in xenografts (Giovanella et al., 1989, 1991). CPT inhibits the enzyme DNA topoisomerase I, initially by noncovalent binding and subsequently by stabilization of the complex through a nucleophilic attack by the enzyme at the acyl position of the CPT lactone ring (Hertzberg et al., 1989). In early clinical trials, CPT was formulated as a water-soluble CPT-Na^+ (Moertel et al., 1972). However, it was later reported that the lactone E-ring is important for cytotoxicity and that the open-ring carboxylated CPT-Na^+ is inactive. The lactone of CPT is converted to carboxylate in a pH-dependent equilibrium (Fig. 1) (Fassberg and Stella, 1992). To overcome the solubility and stability problems of CPT, several approaches have been investigated. Water-soluble CPT analogs have been prepared but the majority of them were less potent in assays both in vitro and in vivo than the parent drug (Wall and Wani, 1995). Therefore, the development of adequate drug carriers is gaining increasing attention. These include methods such as conjugation to polymers (Zamai et al., 2003; Singer et al., 2001), intercalation into liposomes (Burke et al., 1992; Cortesi et al., 1997), solubilization in microemulsions (Cortesi et al., 1997), formation of inclusion complexes with cyclodextrins (Kang et al., 2002) and entrapment in microspheres (Shenderova et al., 1999; Tong et al., 2003). However, concerning long circulation carriers of CPT in blood stream, there was not enough information.

Drug carriers with longer retention time in the blood stream can be delivered to solid tumors site by a passive

* Corresponding author. Tel.: +81 3 5498 5048; fax: +81 3 5498 5048.
E-mail address: yoshie@hoshi.ac.jp (Y. Maitani).

0378-5173/$ – see front matter © 2005 Elsevier B.V. All rights reserved.
doi:10.1016/j.ijpharm.2005.10.030

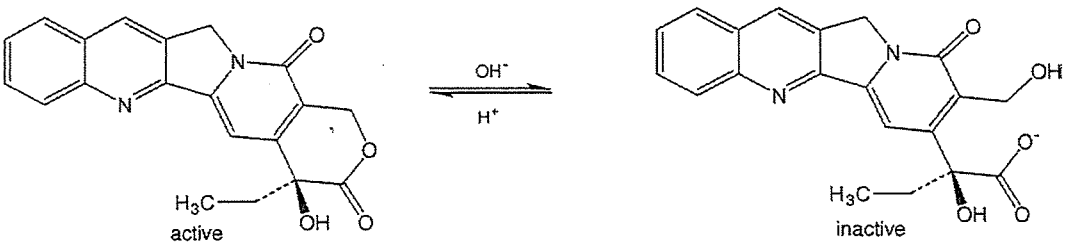

Fig. 1. The structure of camptothecin and equilibrium reaction between the active form and inactive form.

targeting mechanism based on the enhanced permeability and retention effect (EPR effect) (Matsumura and Maeda, 1986; Maeda, 2000; Maeda et al., 2000). Recently, antitumor drug targeting using polymeric micelle carrier systems was achieved with doxorubicin (adriamycin, ADR) using poly(ethylene glycol)–poly(aspartate derivative) block copolymer PEG-P(Asp(R)) (Yokoyama et al., 1987, 1990, 1991, 1998). As a result of selective delivery to tumor site by the EPR effect, dramatically enhanced antitumor effects were obtained in vivo (Yokoyama et al., 1999). In this system, ADR was chemically conjugated to the aspartic acid residue of the block copolymer as hydrophobic species for micelle formation and enhance the physical incorporation of ADR in the inner core. However, the chemically conjugated ADR did not play a role in the expression of anticancer activity (Yokoyama et al., 1999, 1998). Only the physically incorporated ADR expressed selective anticancer activity by being recruited to solid tumor sites.

In previous studies, we reported polymeric micelle system for incorporation of CPT, in which CPT incorporation efficiency and CPT-loaded micelles stability were improved by modification of a hydrophobic segment of the PEG-P(Asp) (Yokoyama et al., 2004; Opanasopit et al., 2004). Chemical structure of block copolymers would largely influence to the stability of polymeric micelles in blood stream. In this study, the in vivo circulation stability of CPT-loaded micelles was evaluated in terms of copolymer composition (PEG length, Asp unit number, ester groups, and esterification degree) and feeding ratio of the drug to copolymer, and compared with incorporation stability of CPT. CPT-loaded micelles with a stable copolymer composition enhanced the circulation time of CPT in the blood stream, which will contribute to recruitment to solid tumor sites.

2. Materials and methods

2.1. Materials

Poly(ethylene glycol)–poly(β-benzyl L-aspartate) block copolymer (PEG–PBLA) was synthesized as described previously (Yokoyama et al., 1992). (s)-(+)-CPT was purchased from Aldrich Chem. Co. (Milw., WI, USA). 1,8-Diazabicyclo[5,4,0]7-undecene (DBU), high performance liquid chromatography (HPLC) grade acetonitrile and triethylamine acetate were purchased from Wako Pure Chemicals, (Tokyo, Japan). *N,N*-dimethylformamide (DMF) was dried over a molecular sieve (4A), and distilled under reduced pressure. Other chemicals were of reagent grade.

2.2. Synthesis of diblock copolymers (PEG–PBLA and its derivatives)

Poly(ethylene glycol)–poly(β-benzyl L-aspartate) block copolymer (PEG–PBLA) was synthesized by ring-opening polymerization of benzyl L-aspartate *N*-carboxy anhydride from a terminal primary amino group of α-methyl-ω-amino-poly(oxyethylene), and poly(ethylene glycol)–poly(aspartic acid) block copolymer (PEG-P(Asp)) was obtained by alkaline hydrolysis of PEG–PBLA as reported previously (Yokoyama et al., 1992). Briefly, PEG–PBLA was dispersed in a measured volume of 0.5N NaOH that contained 1.5 mol. equivalents of NaOH to the benzyl aspartate residue of PEG–PBLA. With stirring at room temperature, the solution became homogeneous in approximately 15 min. Then, 6N HCl was added (10 mol. equivalents of HCl to the benzyl aspartate residue) to the solution, and this solution was dialyzed against 0.1N HCl, followed by distilled water using a SpectraPor®-6 dialysis membrane (MWCO: 1000). PEG-P(Asp) block copolymer was obtained by freeze-drying the dialyzed solution.

Esterification of the aspartic acid residues was achieved through nucleophilic substitution of the carboxyl group with a halogen compound using 1,8-diazabicyclo [5,4,0] 7-undecene (DBU) as a catalyst, as reported previously (Opanasopit et al., 2004). PEG-P(Asp) block copolymer was dissolved in DMF and added to a halogen compound or a mixture of two halogen compounds (benzyl bromide, *n*-butyl bromide, or lauryl bromide) and DBU. The reaction mixture was stirred at 50 °C for ca. 16 h. Then, it was poured into a 10-fold volume excess of diethyl ether, and the precipitated polymer was collected by filtration, followed by washing with diethyl ether and drying. In order to remove DBU from the polymer products, polymers were dissolved in DMSO and added to 6N HCl that was much excess equivalents to the aspartic acid residue of the block copolymer. Then, this solution was dialyzed against distilled water, and freeze-dried.

Ester contents of the block copolymers were determined in ^{1}H NMR spectra by comparing the methylene protons of the hydrophilic PEG block and protons of the hydrophobic moieties of the poly(aspartate) block.

2.3. Preparation of CPT-loaded micelles and CPT solution

CPT was incorporated into polymeric micelles by an evaporation method as reported previously (Opanasopit et al., 2004). Briefly, CPT (0.05, 0.1, 0.2, or 0.4 (CPT/polymer, w/w)) was

dissolved in a mixture of chloroform (1 ml per 1 mg CPT) and acetonitrile (0.67 ml per 1 mg CPT), and added to 5 mg of block copolymer. The solvent was removed by evaporation in a nitrogen gas flow. Then, 3 ml of distilled water was added and sonicated for 2 min using a probe type sonicator model VC 100 (Sonics & Materials Inc., Newtown, Connecticut, USA) equipped with a standard 6 mm probe in a cycle of sonication for 0.5 s and standby for 0.5 s at 80 °C. The solution obtained was centrifuged at 1400 × *g* for 10 min. Subsequently, the supernatant was collected and filtered through a 1 μm pore-sized nylon filter (Puradisc 25NYL, 6751-2510, Whatman, Clifton, New Jersey, USA). CPT-loaded polymeric micelles were kept in a freezer at −20 °C until animal experiments.

The CPT solution was prepared by dissolving CPT (13 mg) in 50 ml of polyethylene glycol 400, propylene glycol and polysorbate 80 (40:50:2, volume ratio) (Yang et al., 1999).

2.4. Determination of CPT content and particle size of micelles

CPT-loaded micelles were dissolved in a mixture of DMSO:H_2O (9:1). The amount of CPT incorporated into polymeric micelles was determined by UV–vis absorption at 365 nm. The incorporation efficiency was calculated as the percentage share of the initial drug used in the preparation for incorporation into the micelles. The mean particle diameters were determined using a dynamic light scattering particle size analyzer (DLS-7000, Otsuka Electronics, Osaka, Japan) at 25 °C by diluting dispersion to an appropriate volume with water.

2.5. Incorporation stability of CPT-loaded micelles evaluated by GPC

The incorporation stability of CPT-loaded micelles was evaluated by gel-permeation chromatography (GPC) as described previously (Yokoyama et al., 1994). GPC was carried out using a Tosoh HPLC system SC-8010 equipped with a Tosoh TSKgel G3000PW_{XL} column. Distilled water was used as the eluent at a flow rate of 1 ml/min at 40 °C. Sample solutions (50 μl) were injected into the column. The detection was performed by measuring absorption at 351 nm for CPT using a Tosoh UV-8010 detector and a refractive index (RI) detector for polymers. A micelle peak was observed at the gel-exclusion volume. GPC with UV detection allowed us to evaluate the nature of the polymeric micelles obtained and the degree of drug incorporation. The peak area detected by UV absorption represents the amount of CPT loaded into the micelles. Therefore, the ratio of the micelle peak area/CPT concentration of the injected sample [CPT] was evaluated as the incorporation stability of CPT-loaded micelles. The small values of the peak area/[CPT] means that most of the CPT was adsorbed to the GPC column by hydrophobic interactions due to unstable packaging of CPT in the micelles. When this ratio was large, CPT was more stably incorporated into micelles.

2.6. Measurement of CPT concentration in plasma

CPT-loaded micelles were intravenously (i.v.) administered to male ddY mice (weighing 18–20 g, Tokyo Laboratory Animal Science Co., Ltd., Tokyo, Japan) via lateral tail veins at a dose of 2.5 mg/kg. For each sampling point, three mice were injected with CPT-loaded micelles. At various time points after the administration, approximately 1 ml of blood was withdrawn using a heparinized syringe and centrifuged at 15,300 × *g* for 4 min to obtain the plasma. Immediately after that, 0.15 M aqueous phosphoric acid was added to the plasma and mixed vigorously (Onishi et al., 2003). CPT was extracted with chloroform: methanol (4:1 volume ratio). After centrifugation of the mixture at 15,300 × *g* for 4 min, 25 μl of the chloroform: methanol layer was directly injected into the HPLC system to determine the concentration of CPT. This operation gave the total concentration of free and incorporated CPT in micelles.

The HPLC analysis was performed at room temperature. A Shimadzu LC-10AT (Shimadzu Corp., Japan) apparatus equipped with a Shimadzu RF-$10A_{XL}$ fluorescence detector in which the excitation and emission wavelength was set at 369 and 426 nm, respectively, was used. A Tosoh TSK-gel ODS-80Ts column (150 mm × 4.6 mm i.d.) was also used. The mobile phase was composed of 23:77 (v/v) acetonitrile–triethylamine acetate buffer (1% (v/v) adjusted to pH 5.5 with glacial acetic acid), and the flow rate was set at 1 ml/min (Warner and Burke, 1997). The areas under the concentration curve (from 0 to 24 h; AUC) were calculated using the trapezoid method.

2.7. Statistical analysis

The results were analyzed statistically using the Student's *t*-test. When comparisons between groups yielded a value for $P < 0.05$, the difference between those groups was considered significant.

3. Results and discussion

3.1. Characterization

Polymeric micelles with a particle diameter of less than 100 nm and a PEG-coated surface have been found to well avoid entrapment by the reticuloendothelial system (RES) and to well leak in diseased areas with highly permeable blood vessels, resulting in passive targeting to the diseased sites (Yokoyama et al., 1993; Kwon et al., 1994); this is known as the EPR effect. In order to sufficiently acquire this EPR effect, we examined the effect of various polymers on the CPT incorporation stability and evaluated the pharmacokinetic profile of CPT-loaded micelles.

Chemical structure of poly(ethylene glycol)–poly(aspartate ester) block copolymer (PEG-P(Asp(R))) is shown in Fig. 2. The block copolymers are coded by the chain lengths of both blocks, the name of the hydrophobic group, and the degree of esterification as summarized in Table 1. For example, 5-27 Bz44 represents a block copolymer composed of a PEG block of molecular weight 5000 and a P(Asp) block possessing 27 units of aspartic acid, in which 44%

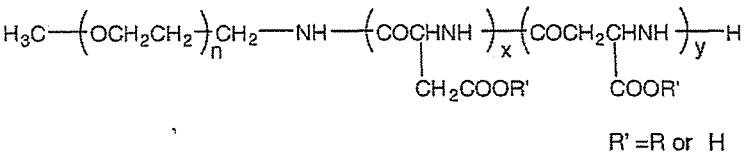

Fig. 2. Chemical structure of poly(ethylene glycol)–poly(aspartate ester) block copolymer (PEG-P(Asp(R))).

Table 1
Poly(ethylene glycol)–poly(aspartate ester) diblock copolymers (PEG-P(Asp(R)))

Code	PEG (MW)	Asp[a] ester ($x+y$ unit)	Ester (R)	Esterification (%)
5-27 Bz44	5000	27.1	Benzyl	44
5-27 Bz57	5000	27.1	Benzyl	57
5-27 Bz75	5000	27.1	Benzyl	75
5-52 Bz74	5000	52.0	Benzyl	74
12-25 Bz71	12000	27.1	Benzyl	71
12-50 Bz63	12000	50.0	Benzyl	63
5-27 *n*-Bu6 + Bz57	5000	27.1	*n*-Butyl + benzyl	6 + 57
5-27 Lau5 + Bz58	5000	27.1	Lauryl + benzyl	5 + 58

[a] Asp: aspartate.

of the aspartic acid residues are esterified with a benzyl group.

3.2. Ester groups of polymers

To determine the structural requirements for stability, polymers with three kinds of ester groups were synthesized. The incorporation of CPT into polymeric micelles was successfully achieved by the evaporation method which provided high CPT yields (Opanasopit et al., 2004). Table 2 shows the effect of ester groups (benzyl and mixture (benzyl + lauryl, benzyl + *n*-butyl)) on the entrapment efficiency, incorporation stability evaluated by GPC and the % injected dose in plasma after 4 h. When the ratio of micelles peak area/CPT concentration [CPT] was large, the CPT incorporated into the micelles was more stable. CPT micelles of these three ester groups showed similar stability in vitro, but not in vivo. Benzyl polymeric micelles suggested a longer circulation time than *n*-butyl and lauryl ones in spite that the mixture had a more hydrophobic inner core than benzyl. This implies that not only hydrophobicity but also physical factors such as rigidity and π–π interactions of the inner core-forming block contributed to the incorporation, since the lauryl ester (C12) is more hydrophobic than the benzyl ester (C7).

Table 3
Effect of PEG length (5000 or 12,000) and Asp unit (27 or 50) on stability of CPT-loaded micelles at a feeding ratio (CPT/polymer) of 0.4 (w/w)

Code	Peak area/[CPT][a]	% Injected dose in plasma after 4 h[b]
5-27 Bz75	46.5	9.3 ± 1.8
12-25 Bz71	26.5	2.6 ± 0.6
5-52 Bz74	86.1	6.7 ± 0.5
12-50 Bz63	21.9	2.2 ± 0.4
CPT-solution[c]	–[d]	0.04 ± 0.03

[a] Incorporation stability; peak area, evaluated by GPC, was divided by CPT concentration in micelles [CPT] ($n = 1$–2).
[b] Results at a dose of 2.5 mg/kg are given as the mean ± S.D. ($n = 3$).
[c] CPT was dissolved in polyethylene glycol 400:propylene glycol: Tween 80 = 40:58:2 (volume ratio).
[d] Not done.

PEG–PBLA can be handled as benzyl-100% because its aspartic acid residues were fully benzylated. However, in the stability assay using GPC, PEG–PBLA micelles provided much lower incorporation stability than the benzyl-57% block copolymer. This indicates that the conformation and/or configuration of the hydrophobic inner core-forming polymer block contributes to a stable incorporation by providing the appropriate space for CPT.

3.3. PEG length and Asp unit of polymers

To determine the contribution of PEG length and Asp unit to the micelles' stability, four polymeric micelles of Bz with different combinations of PEG length (5000 or 12,000) and Asp units (27 and 50) were prepared (Table 3). Compared with the CPT solution as a control, at both 27 and 50 Asp units, CPT micelles of PEG 5000 showed a longer circulation than those of PEG 12,000 in vivo.

An increase in the chain length of a hydrophobic block at a given chain length of a hydrophilic block causes a decrease in the critical micelle concentration (CMC) (Leibler et al., 1983). In contrast, the ADR-loaded PEG-P(Asp(ADR)) micelles, pos-

Table 2
Effect of ester group of polymer 5-27 (PEG 5000-Asp unit 27) on stability of CPT-loaded micelles at a feeding ratio (CPT/polymer) of 0.1 (w/w)

Code	Esterification (%) of diblock copolymer	Entrapment efficiency (%)[a]	Peak area/[CPT][b]	% Injected dose in plasma after 4 h[c]
5-27 *n*-Bu6 + Bz57	*n*-Bu 6 + Bz57	37.8	58.1	0.15 ± 0.08
5-27 Lau5 + Bz58	Lauryl 5 + Bz58	47.5	48.3	0.07 ± 0.03
5-27 Bz57	Bz57	88.6	55.3	7.6 ± 0.8
PEG–PBLA	Bz100	67.7	1.5	–[d]

[a] $n = 1$–2.
[b] Incorporation stability; peak area, evaluated by GPC, was divided by CPT concentration in micelles [CPT] ($n = 1$–2).
[c] Results at a dose of 2.5 mg/kg are given as the mean ± S.D. ($n = 3$).
[d] Not done.

sessing a longer hydrophilic PEG chain and a shorter hydrophobic P(Asp(ADR)) chain circulated longer in blood (Kwon et al., 1993, 1994), accumulated more in tumors (Kwon et al., 1994), and showed greater antitumor activity (Yokoyama et al., 1993). This is a reversed relationship estimated from the CMC phenomenon of block copolymers. This implies that dynamic stability of the polymeric micelles that is defined with a dissociation constant of the micelle structure is more important in vivo than static micelle stability that is defined with CMC values. In this study, at a similar number of the Asp units, the micelles possessing PEG 5000 was found to be more stable than those possessing PEG 12,000 in blood circulation. This fact was opposite to the ADR case. More detailed study is required to elucidate the relationship between in vivo stability and compositions of polymeric micelles by more quantitatively evaluating strength and nature (e.g., degree of contribution of π–π interaction) of interactions utilized for micelle formation and drug incorporation.

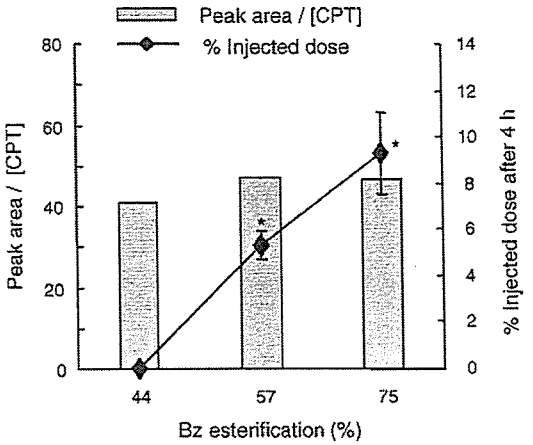

Fig. 3. Effect of esterification of 5-27 Bz on stability of CPT-loaded micelles at a feeding ratio (CPT/polymer) of 0.4 (w/w). The ratio of peak area/[CPT] indicated the incorporation stability of CPT-loaded micelles. Percentage injected dose represents the mean ± S.D., $n=3$. $^{*}P<0.05$; compared with 5-27 Bz44.

3.4. Benzyl ester content in micelles

For the ADR-loaded polymeric micelle system, a larger amount of the chemically conjugated ADR (63 mol% with respect to the aspartic acid residue of the block copolymer) provided more stable circulation in blood of the physically entrapped ADR that exhibited targeted anti-tumor activity than a smaller amount case (41 mol%). In the present study, to determine the contribution of esterification to micelle stability, three kinds of 5-27 micelles with different amounts of Bz were prepared. The mean particle sizes of 5-27 Bz44, Bz57 and Bz75 were 275.8, 182.7 and 196.1 nm, respectively. The effect of esterification of 5-27 Bz on the stability of CPT-loaded micelles at a feeding ratio (CPT/polymer) of 0.4 (w/w) was examined by GPC and by measuring the % injected dose in plasma after 4 h (Fig. 3). When the benzyl ester content was increased from 44 to 75%, the stability of polymeric micelles was similar in vitro, but CPT-loaded micelles of 5-27 Bz44 showed poor circulation stability. CPT-loaded micelles were able to maintain stability in vivo on esterification of more than 57% of the polymer. As showing Table 2, PEG–PBLA (Bz100%) micelles were not stable in in vitro. Therefore, stable micelle formulation was obtained when the esterification ratio of Bz was appropriate (57–75%). This finding corresponded well that CPT release rate from the micelles for PEG–PBLA or 5-27 Bz44 was faster than that for 5-27 Bz75, when incubated in PBS at 37 °C (Opanasopit et al., 2004). The result suggested that the contribution of π–π interaction between aromatic groups of CPT molecules could be maintained, when the degree of esterification of Bz was more than 57%.

3.5. Feeding ratio of CPT/polymer in micelle

To investigate the influence of feeding ratio on the micelle characteristics, CPT-loaded polymeric micelles were prepared at the different feeding ratio (0.05, 0.1, 0.2 and 0.4 (w/w)). Fig. 4 shows the entrapment efficiency, mean particle size, and the incorporation and circulation stability of CPT-loaded 5-27 Bz57 polymeric micelles, respectively. Regardless of feeding

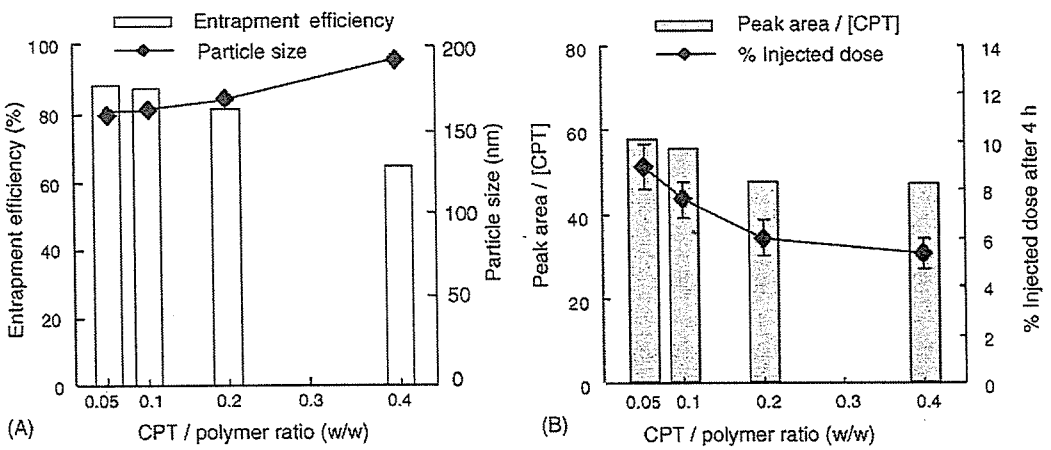

Fig. 4. Effect of feeding ratio (CPT/5-27 Bz57 polymer, w/w) on entrapment efficiency, particle size (A), and the incorporation (peak area/[CPT]) and circulation stability of CPT-loaded micelles (B). Particle size and % injected dose represent the mean ± S.D., $n=3$.

ratio of CPT/polymer, obtained CPT-loaded micelles showed similar particle size (150–200 nm) and stability of in vitro and in vivo (5–10% injected dose after 4 h). CPT-loaded 5-27 Bz57 micelles were stable in vivo even if the amount of CPT in the polymer was increased. In the case of ADR-loaded polymeric micelles, 21 w/w% ADR was physically incorporated whereas intact ADR, having antitumor activity, accounted for only 5 w/w% (Yokoyama et al., 1999). The feeding ratio of 0.4 (w/w) CPT/polymers corresponds to more than 20 w/w% of CPT in obtained micelles, where CPT was incorporated in the active lactone form (>95%). Therefore, this system will be able to deliver a massive amount of intact drug to the targeted site.

3.6. Plasma concentration–time profiles

As a stable formulation of CPT-loaded micelle was obtained using the polymer with 57–75% Bz esterification at a feeding ratio (CPT/polymer) of 0.4 (w/w), the plasma pharmacokinetics of the CPT-loaded 5-27 Bz63 polymeric micelles was compared with unstable formulations such as 5-27 Bz44 and CPT solution (Fig. 5). CPT-loaded 5-27 Bz63 and 5-27 Bz44 micelles at a feeding ratio (CPT/polymer) of 0.4 (w/w) showed 275.8 ± 14.8 and 276.5 ± 24.8 nm in size, respectively. As expected from Fig. 3, a long-circulation was obvious for the CPT in 5-27 Bz63 compared to 5-27 Bz44 and CPT solution. This finding corresponded with the result of CPT release from polymeric micelles in vitro, showing the slower CPT release from 5-27 Bz75 than 5-27 Bz44 in PBS at 37 °C (Opanasopit et al., 2004). Hydrophilic PEG chains exposed to the aqueous surroundings may prevent the adsorption of blood proteins onto the micelles' surface and from being cleared through RES. In spite of similar particle size, the stable polymeric micelle (Bz63) showed about a 17-fold lower clearance value than the unstable one (Bz44) (Table 4). This finding suggested that the stable incorporation of CPT into micelles by the hydrophobic interaction of intact CPT with inner core of polymeric micelles, e.g., π–π interactions of the benzyl ester, may be important in the circulation stability.

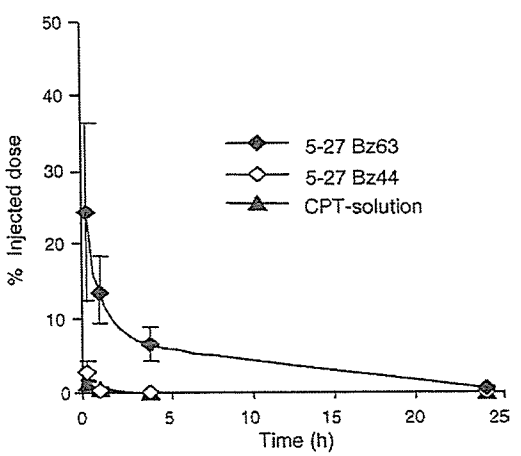

Fig. 5. Plasma concentration–time curves of the CPT-loaded 5-27 Bz (44 or 63) micelles and CPT solution following i.v. administration at a dose of 2.5 mg CPT/kg in ddY mice. The feeding ratio (CPT/polymer) was 0.4 (w/w). Results are given as the mean ± S.D., $n = 3$.

Table 4
Pharmacokinetic parameters after i.v. administration of CPT-loaded 5-27 Bz (44 or 63) micelles in mice at a dose of 2.5 mg/kg

Code	AUC (μg h ml^{-1})	Clearance (ml h^{-1} g^{-1})	
5-27 Bz63	47.0 ± 2.4	0.053 ± 0.003	**
5-27 Bz44	2.7 ± 0.02	0.91 ± 0.007	

The feeding ratio (CPT/polymer) was 0.4 (w/w). AUC: area under the concentration–time curve from 0 to 24 h. Results are given as the mean±S.D. ($n = 3$).
** $P < 0.01$

4. Conclusion

The stable formulation of CPT-loaded micelles in vivo strongly depended on the amount of benzyl esters and length of the PEG of polymers, more so than in vitro. A stable formulation of CPT-loaded micelles was obtained using PEG-P(Asp) with a PEG of 5000 (MW), 27 Asp units, and 57–75% benzyl esterification. The CPT-loaded micelles are potentially delivered to tumor sites owing to an extended circulation in the blood stream.

Acknowledgments

We are grateful to Ms. C. Kanai, Ms. S. Katayama and Ms. C. Fujita for their technical assistance.

References

Burke, T.G., Staubus, A.E., Mishra, A.K., 1992. Liposomal stabilization of camptothecin's lactone ring. J. Am. Chem. Soc. 114, 8318–8319.
Cortesi, R., Esposito, E., Maietti, A., Menegatti, E., Nastruzzi, C., 1997. Formulation study for the antitumor drug camptothecin: liposomes, micellar solution, and a microemulsion. Int. J. Pharm. 159, 95–103.
Fassberg, J., Stella, V.J., 1992. A kinetic and mechanistic study of the hydrolysis of camptothecin and some analogues. J. Pharm. Sci. 81, 676–684.
Giovanella, B.C., Hinz, H.R., Kozielski, A.J., Stehlin Jr., J.S., Silber, R., Potmesil, M., 1991. Complete growth inhibition of human cancer xenografts in nude mice by treatment with 20-(*S*)-camptothecin. Cancer Res. 51, 3052–3055.
Giovanella, B.C., Stehlin, J.S., Wall, M.E., Wani, M.C., Nicholas, A.W., Liu, L.F., Silber, R., Potmesil, M., 1989. DNA topoisomerase I-targeted chemotherapy of human colon cancer in xenografts. Science 246, 1046–1048.
Hertzberg, R.P., Caranfa, M.J., Hecht, S.M., 1989. On the mechanism of topoisomerase I inhibition by camptothecin: evidence for binding to an enzyme-DNA complex. Biochemistry 28, 4629–4638.
Kang, J., Kumar, V., Yang, D., Chowdhury, P.R., Hohl, R.J., 2002. Cyclodextrin complexation: influence on the solubility, stability, and cytotoxicity of camptothecin, an antineoplastic agent. Eur. J. Pharm. Sci. 15, 163–170.
Kwon, G., Suwa, S., Yokoyama, M., Okano, T., Sakurai, Y., Kataoka, K., 1994. Enhanced tumor accumulation and prolonged circulation times of micelle-forming poly(ethylene oxide-aspartate) block copolymer-adriamycin conjugates. J. Control. Rel. 29, 17–23.
Kwon, G.S., Yokoyama, M., Okano, T., Sakurai, Y., Kataoka, K., 1993. Biodistribution of micelle-forming polymer-drug conjugates. Pharm. Res. 10, 970–974.
Leibler, L., Orland, H., Wheeler, J.C., 1983. Theory of critical micelle concentration for solutions of block copolymers. J. Chem. Phys. 79, 3550–3557.
Maeda, H., 2000. The enhanced permeability and retention (EPR) effect in tumor vasculature. The key role of tumor-selective macromolecular drug targeting. Adv. Enzyme Regul. 41, 189–207.

Maeda, H., Wu, J., Sawa, T., Matsumura, Y., Hori, K., 2000. Tumor vascular permeability and the EPR effect in macromolecular therapeutics: a review. J. Control. Rel. 65, 271–284.

Matsumura, Y., Maeda, H., 1986. A new concept for macromolecular therapeutics in cancer chemotherapy: mechanism of tumoritropic accumulation of proteins and the antitumor agent smancs. Cancer Res. 46, 6387–6392.

Moertel, C.G., Schutt, A.J., Reitemeier, R.J., Hahn, R.G., 1972. Phase II study of camptothecin (NSC-100880) in the treatment of advanced gastrointestinal cancer. Cancer Chemother. Rep. 56, 95–101.

Onishi, H., Machida, Y., Machida, Y., 2003. Antitumor properties of irinotecan-containing nanoparticles prepared using poly(DL-lactic acid) and poly(ethylene glycol)-block-poly(propylene glycol)-block-poly(ethylene glycol). Biol. Pharm. Bull. 26, 116–119.

Opanasopit, P., Yokoyama, M., Watanabe, M., Kawano, K., Maitani, Y., Okano, T., 2004. Block copolymer design for camptothecin incorporation into polymeric micelles for passive tumor targeting. Pharm. Res. 21, 2001–2008.

Shenderova, A., Burke, T.G., Schwendeman, S.P., 1999. The acidic microclimate in poly(lactide-co-glycolide) microspheres stabilizes camptothecins. Pharm. Res. 16, 241–248.

Singer, J.W., Bhatt, R., Tulinsky, J., Buhler, K.R., Heasley, E., Klein, P., de Vries, P., 2001. Water-soluble poly-(L-glutamic acid)-Gly-camptothecin conjugates enhance camptothecin stability and efficacy in vivo. J. Control. Rel. 74, 243–247.

Tong, W., Wang, L., D'Souza, M.J., 2003. Evaluation of PLGA microspheres as delivery system for antitumor agent-camptothecin. Drug Dev. Ind. Pharm. 29, 745–756.

Wall, M.E., Wani, M.C., 1995. Camptothecin and analogs: from discovery to clinic. In: Potmesil, M., Pinedo, H. (Eds.), Camptothecin: New Anticancer Agents. CRC Press, Boca Raton, FL, pp. 21–41.

Wall, M.E., Wani, M.C., Cook, C.E., Palmer, K.H., Mcphail, A.T., Sim, G.A., 1966. Plant antitumor agents. I. The isolation and structure of camptothecin, a novel alkaloidal leukemia and tumor inhibitor from Camptotheca acuminate. J. Am. Chem. Soc. 88, 3888–3890.

Warner, D.L., Burke, T.G., 1997. Simple and versatile high-performance liquid chromatographic method for the simultaneous quantitation of the lactone and carboxylate forms of camptothecin anticancer drugs. J. Chromatogr. B: Biomed. Sci. Appl. 691, 161–171.

Yang, S.C., Lu, L.F., Cai, Y., Zhu, J.B., Liang, B.W., Yang, C.Z., 1999. Body distribution in mice of intravenously injected camptothecin solid lipid nanoparticles and targeting effect on brain. J. Control. Rel. 59, 299–307.

Yokoyama, M., Fukushima, S., Uehara, R., Okamoto, K., Kataoka, K., Sakurai, Y., Okano, T., 1998. Characterization of physical entrapment and chemical conjugation of adriamycin in polymeric micelles and their design for in vivo delivery to a solid tumor. J. Control. Rel. 50, 79–92.

Yokoyama, M., Inoue, S., Kataoka, K., Yui, N., Sakurai, Y., 1987. Preparation of adriamycin-conjugated poly(ethylene glycol)-poly(aspartic acid) block copolymer. A new type of polymeric anticancer agent. Die Makromolekulare Chemie Rapid Commun. 8, 431–435.

Yokoyama, M., Kwon, G.S., Okano, T., Sakurai, Y., Seto, T., Kataoka, K., 1992. Preparation of micelle-forming polymer-drug conjugates. Bioconjug. Chem. 3, 295–301.

Yokoyama, M., Kwon, G.S., Okano, T., Sakurai, Y., Ekimoto, H., Okamoto, K., Mashiba, H., Seto, T., Kataoka, K., 1993. Composition-dependent in vivo antitumor activity of adriamycin-conjugated polymeric micelle against murine colon adenocarcinoma 26. Drug Del. 4, 11–19.

Yokoyama, M., Kwon, G.S., Okano, T., Sakurai, Y., Naito, M., Kataoka, K., 1994. Influencing factors on in vitro micelle stability of adriamycin-block copolymer conjugates. J. Control. Rel. 28, 59–65.

Yokoyama, M., Miyauchi, M., Yamada, N., Okano, T., Sakurai, Y., Kataoka, K., Inoue, S., 1990. Characterization and anticancer activity of the micelle-forming polymeric anticancer drug adriamycin-conjugated poly(ethylene glycol)–poly(aspartic acid) block copolymer. Cancer Res. 50, 1693–1700.

Yokoyama, M., Okano, T., Sakurai, Y., Ekimoto, H., Shibazaki, C., Kataoka, K., 1991. Toxicity and antitumor activity against solid tumors of micelle-forming polymeric anticancer drug and its extremely long circulation in blood. Cancer Res. 51, 3229–3236.

Yokoyama, M., Okano, T., Sakurai, Y., Fukushima, S., Okamoto, K., Kataoka, K., 1999. Selective delivery of adriamycin to a solid tumor using a polymeric micelle carrier system. J. Drug Target. 7, 171–186.

Yokoyama, M., Opanasopit, P., Okano, T., Kawano, K., Maitani, Y., 2004. Polymer design and incorporation methods for polymeric micelle carrier system containing water-insoluble anti-cancer agent camptothecin. J. Drug Target., 373–384.

Zamai, M., VandeVen, M., Farao, M., Gratton, E., Ghiglieri, A., Castelli, M.G., Fontana, E., D'Argy, R., Fiorino, A., Pesenti, E., Suarato, A., Caiolfa, V.R., 2003. Camptothecin poly[*n*-(2-hydroxypropyl) methacrylamide] copolymers in antitopoisomerase-I tumor therapy: intratumor release and antitumor efficacy. Mol. Cancer Ther. 2, 29–40.